Geophys. J. Int. (2009) **179,** 850–872 doi: 10.1111/j.1365-246X.2009.04346.x

Palaeomagnetism of the 2054 Ma Bushveld Complex (South Africa): implications for emplacement and cooling

Shawn Letts,[1,2] Trond H. Torsvik,[1,3,4] Susan J. Webb[1] and Lewis D. Ashwal[1]

[1]*School of Geosciences, University of Witwatersrand, WITS* 2050, *South Africa. E-mail: trond.torsvik@ngu.no*
[2]*Anglo American, PO Box* 61587, *Marshalltown, Johannesburg* 2107, *South Africa*
[3]*Centre for Geodynamics, Geological Survey of Norway,* N-7491 *Trondheim, Norway*
[4]*Physics of Geological Processes, University of Oslo, Norway*

Accepted 2009 July 26. Received 2009 July 25; in original form 2009 February 8

SUMMARY

The Kaapvaal Craton (South Africa) was the host of several major magmatic events around 2000 Ma, including the Bushveld Complex, the world's largest known layered mafic intrusion ($\sim$0.5–1 $\times$ 10^6 km^3). The Bushveld Complex has been the subject of numerous palaeomagnetic studies, which yielded a large spread in palaeomagnetic pole positions for the different Zones, and interpreted to indicate that the Bushveld Complex was emplaced and cooled over a time span of $\sim$50 million years. New palaeomagnetic data collected from 100 sites (996 drill-cores) from all Zones of the Rustenburg Layered Suite of the Bushveld Complex, yield exceptional palaeomagnetic results with high unblocking (HB) components carried by magnetite. Comparable palaeomagnetic poles from all Zones (mean pole: latitude = 19.2°N, longitude = 030.8°E, A95 = 5.8°) [correction made after online publication 22 September 2009: the mean pole values have been corrected] eliminates the previously noted large spread in poles, and this observation concurs with precise age data that constrain the time period of emplacement of the Bushveld Complex to a few million years at around 2054 Ma. Bedding-corrected HB components from all zones produced better directional groupings, which together with at least seven reversals, strongly points to a primary magnetic signature. This imply that cooling of the Bushveld Complex below the blocking-temperature of magnetite ($<$580 °C) occurred in a near-horizontal position, and based on the maximum observed reversal rates in the geological history ($\sim$5 Ma^{-1}), we estimate a *minimum* cooling-interval for the Bushveld Complex of 1.4 million years.

Key words: Palaeomagnetism applied to geologic processes; Reversals: process, timescale, magnetostratigraphy; Large igneous provinces; Africa.

1 INTRODUCTION

The 2054.4 $\pm$ 1.3 Ma Bushveld Complex (Scoates & Friedman 2008) in northern South Africa (Fig. 1), is the world's largest known layered intrusion and contains the majority of the world's resources of platinum group elements (PGE), chromium and vanadium (Lee 1996). The complex as a whole is composed of five major magmatic suites: the Rooiberg Volcanic Suite (Buchanan *et al.* 2002): the Rustenburg Layered Suite (RLS), marginal pre- and syn-Bushveld sills and intrusions (Frick 1973; Sharpe 1981), the Roshoop Granophyre Suite (Walraven 1985) and the Lebowa Granite Suite (Walraven & Hattingh 1993).

The Rustenburg Layered Suite (RLS), constituting the layered mafic rocks of the Bushveld Complex, and the subject of study for this paper, occurs in four discrete regions or Lobes (Fig. 1): The Western Lobe that extends in an arc from near Pretoria westwards to Rustenburg and is cross-cut by the Pilanesberg alkaline complex, to and along the southern flank of the Makoppa Dome of the Archaean granitiods and gneisses; a south-eastern (Bethal) Lobe, which is largely covered by Mesozoic rocks (not shown in Fig. 1); an Eastern Lobe that extends in a northward arc west of Belfast up to Atok, and a Northern Lobe that extends south of Mokopane to Villa Nora (Tankard *et al.* 1982). The Far Western Lobe extends the Western Lobe another $\sim$100 km west of the Pilanesberg, and consists of scattered sills of limited depth extent. Further west ($\sim$200 km) is the poorly exposed Molopo Farms Complex which is a layered mafic intrusion of the same age as the Bushveld Complex extending for $\sim$100 km north-south and $\sim$200 km east-west.

The RLS has been stratigraphically subdivided by SACS (1980) into five Zones based on cumulus mineral assemblages. The Marginal Zone comprises fine-grained plagioclase-orthopyroxene cumulates. The Lower Zone is dominated by olivine-bearing cumulates, including harzburgite, dunite and orthopyroxenite. The Critical Zone, characterized by the regular layering of dunites, harzburgites, pyroxenites, chromitites, norites and anorthosites. It is the carrier of two of the world's largest platinum-bearing ore bodies,

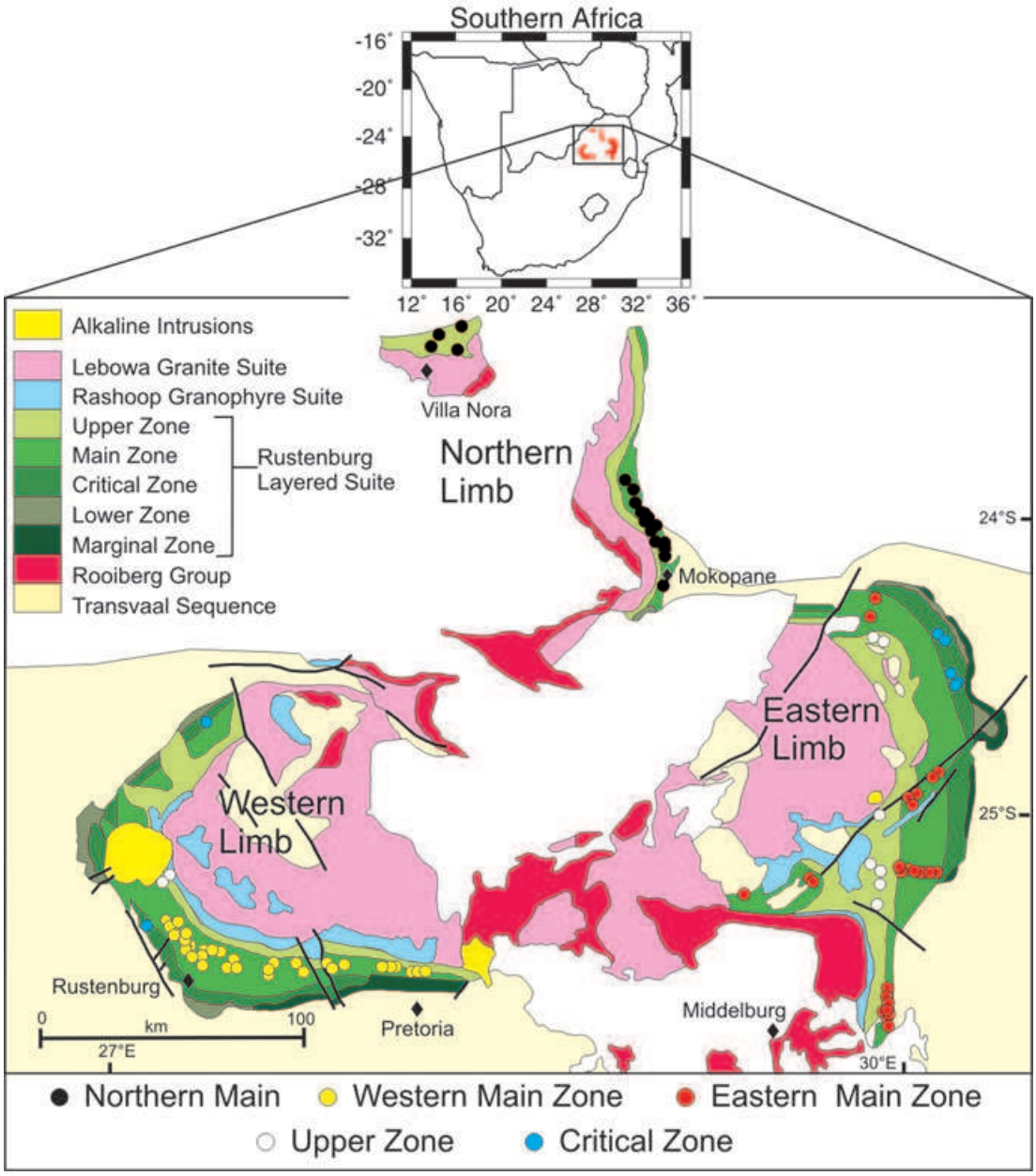

Figure 1. Simplified geological map of the Bushveld Complex, including the mafic Zones (Rustenburg Layered Suite) and felsic phases (Lebowa Granite Suite, Rooiberg group and Rashoop Granophyre Suite) after Cairncross & Dixon (1995).

the Upper Group 2 Chromitite (UG2) and the Merensky Reef, as well as a number of chromite reserves within the Lower (LG), Middle (MG) and Upper (UG) Group chromitite layers (Hatton & Von Gruenewaldt 1987). The Main Zone comprises an approximately 2.5 km thick succession of dominantly gabbronoritic rocks, and the Upper Zone consists of magnetite gabbro (and olivine diorite in the Eastern Lobe).

In general the layers of the RLS for the Eastern and Western Lobes dip towards the centre of the complex, usually at low angles between 10° and 25°. In the northern Lobe, rocks dip towards the west and can display dips as steep as 60° in the vicinity of Villa Nora (Tankard *et al.* 1982).

Geochronological data obtained from the felsic rocks associated with the Bushveld Complex have bracketed the age of the RLS between 2060 ± 2 Ma (Walraven 1997) and 2054.4 ± 1.8 Ma (Walraven & Hattingh 1993). The RLS itself has been dated at 2058.9 ± 0.8 Ma using U-Pb isotopes from newly grown titanite found in calc-silicate xenoliths (Buick *et al.* 2001). An $^{40}Ar/^{39}Ar$ biotite age of 2044.1 ± 2.9 was reported from the UG2 layer (Nomade *et al.* 2004), but these authors concluded that this age was due to a miscalibration of the $^{40}Ar/^{39}Ar$ system. By applying an *ad hoc* correction, they obtained the same age as determined by Buick *et al.* (2001), and concluded that the RLS experienced a very rapid cooling (1000°C Myr^{-1}) from 700° to <500°C. The most recent U-Pb (zircon) age dates RLS (Merensky reef) to 2054.4 ± 1.3 Ma (Scoates & Friedman 2008) and we use this age in our study.

Over the past 40 years the Bushveld Complex has been the subject of numerous studies, including an initial palaeomagnetic investigation in 1959 followed by five papers in the early 1980s (Table 1). The first study was completed by Gough & Van Niekerk (1959) on

Table 1. Palaeomagnetic poles and associated 95 per cent confidence ovals (dp/dm) from previous palaeomagnetic studies conducted on the Bushveld Complex.

Study and zone	Pole longitude	Pole latitude	dp	dm
Gough & Van Niekerk (1959): Main Zone (Eastern and Western Lobes)	23°N	36°E	12°	12°
Hattingh (1986c): Critical Zone (Eastern and Western Lobes)	39.5°N	47°E	7.8°	13.1°
Hattingh (1986b): Main Zone Eastern Lobe	17.3°N	35.7°E	5.4°	6.4°
Hattingh (1986a): Main Zone Western Lobe	9.2°N	27.3°E	4.2°	4.9°
Hattingh (1989): Upper Zone (Eastern and Western Lobes)	16.1°N	31.5°E	14.7°	18°
Hattingh & Paul (1994): Main Zone of Northern Lobe	1.6°N	22.3°E	14.7°	15.9°
Hattingh & Paul (1994): Upper Zone of Northern Lobe	7.9°N	359.3°E	44.4°	54.6°

five sites located in the Main Zone of the Eastern and Western Lobes of Bushveld Complex, and produced a single palaeomagnetic pole for the Bushveld Complex. Later studies by Hattingh (1986a,b,c, 1989) analysed samples from 88 sites located in the Eastern and Western Lobes of the Complex. He obtained four palaeomagnetic pole positions: one for the Critical Zone (seven sites from the Western Lobe and one site from the Eastern Lobe), two for the Main zone (one for the Eastern and the other for the Western Lobes) and one for the Upper Zone (six sites in the Eastern Lobe and two sites in the Western Lobe). The latest study by Hattingh & Pauls (1994) sampled 17 sites in the Main and Upper Zones of the Northern Lobe of the Bushveld Complex, yielding one palaeomagnetic pole position for the Main Zone and a palaeomagnetic pole position for the Upper Zone (calculated from a single observation).

The following inconstancies have been found in these palaeomagnetic results:

(1) The RLS was assumed to have been formed in a horizontal attitude (Hattingh 1986a,b,c, 1989, 1995, 1998; Hattingh & Pauls 1994) and that the present attitude was only acquired after the igneous layering had cooled below the Curie temperature for magnetite (∼580 °C). From the five studies conducted, only one (that of the Eastern Main Zone, Hattingh 1986b) passed the fold test of McElhinny (1964). The other four studies are not significant at 95 percent confidence level after restoring the igneous layering to the horizontal. Therefore, the assumption that the Complex was horizontal at the Curie temperature of magnetite has not been statistically shown by these previous studies.

(2) Based on very different palaeomagnetic poles from the Bushveld Complex, defining an apparent polar wander (APW) path of almost 45° in arc length, it was assumed that the different zones of the RLS were emplaced and cooled over a time span of ∼50 Myr This is in contradiction to newly determined precise geochronological data obtained from the felsic rocks associated with the Bushveld Complex, which bracket the Rustenburg Layered Suite between 2060 ± 2 Ma (Walraven 1997) and 2054.4 ± 1.3 Ma (Walraven & Hattingh 1993; Scoates & Friedman 2008), that is less than 6 Myr. The 50 Myr emplacement span also contradicts modelling conducted by Cawthorn & Walraven (1998), which suggests that the Bushveld Complex cooled rapidly and crystallized in about 200 000 years.

Based on the fact that palaeomagnetic equipment and data analysis techniques have improved considerably over the past decades, a simple re-evaluation of the existing data was not sufficient to properly evaluate the palaeomagnetic signature of Bushveld Complex. Thus, a new and comprehensive study was conducted.

2 PALAEOMAGNETIC SAMPLING

Large areas of the Bushveld Complex are covered by considerably thick soil layers (5–15 m), and due to lack of positive topography, exposures and hence sampling localities are generally isolated. This resulted in samples for this study having been obtained from dimension stone quarries, road cuttings, limited stream sections and underground platinum mines; in a few instances samples were obtained from low-lying hill outcrops in the Northern Lobe (see Letts 2007, for more details). Topographic highs were not considered due to these areas being prone to lightning strikes. With the scarcity of suitable sampling locations and the limited number of road and river exposures in the Bushveld Complex, a number of sites sampled in this study are identical to those of Hattingh (1983). A total of 100 sites were sampled throughout the Bushveld Complex (Fig. 1), and the stratigraphic locations of sites are shown in Figs 2 and 3. A grand total of 966 core samples were obtained and subjected to palaeomagnetic analysis, the results of which are discussed further. Sampling and palaeomagnetic results have been broken down into five groups:

2.1 Main Zone, Western Lobe

Palaeomagnetic drill locations were limited to the lowermost stratigraphic units, extending from Pretoria westwards towards the Pilanesburg Complex (Fig. 4a). A total of 30 sites were drilled and sampling included gabbronorites situated at different stratigraphic heights within the Pyramid Gabbronorite sections (Fig. 4b).

2.2 Main Zone, Eastern Lobe

A total of 26 sites were sampled (Fig. 5) and reasonable coverage was obtained throughout the Main Zone in which the SACS (1980) classification of the sub-zones A, B and C (also known as Winnaarshoek Norite-Anorthosite, Leolo Mountain Gabbro-Norite and Mapoch Gabbro-Norite) were sampled (Fig. 5).

2.3 Critical Zone

Outcrops of the Critical Zone produced four viable palaeomagnetic drill-sites. A rather restricted number of suitable surface sites led to samples being obtained from underground platinum mines, where another six sites were sampled. Four mines were visited: Hackney (2 sites, Eastern lobe), Royal Bafokeng resource (BRPM, 2 sites, Western Lobe), Amandelbuilt (Western Lobe) and Modikwa (Eastern Lobe) (Fig. 6a). Coverage of the Critical Zone is imperfect, with large sections of the Zone being un-sampled (Figs 6b and c). In previous studies samples were orientated underground using a magnetic compass; this is hardly recommended as magnetic readings are strongly affected by underground infrastructure (electrical cables, cooling vents and support pillars) and highly magnetic rocks. Before samples could be obtained a reliable method of orientating therefore had to be developed (detailed in Appendix A).

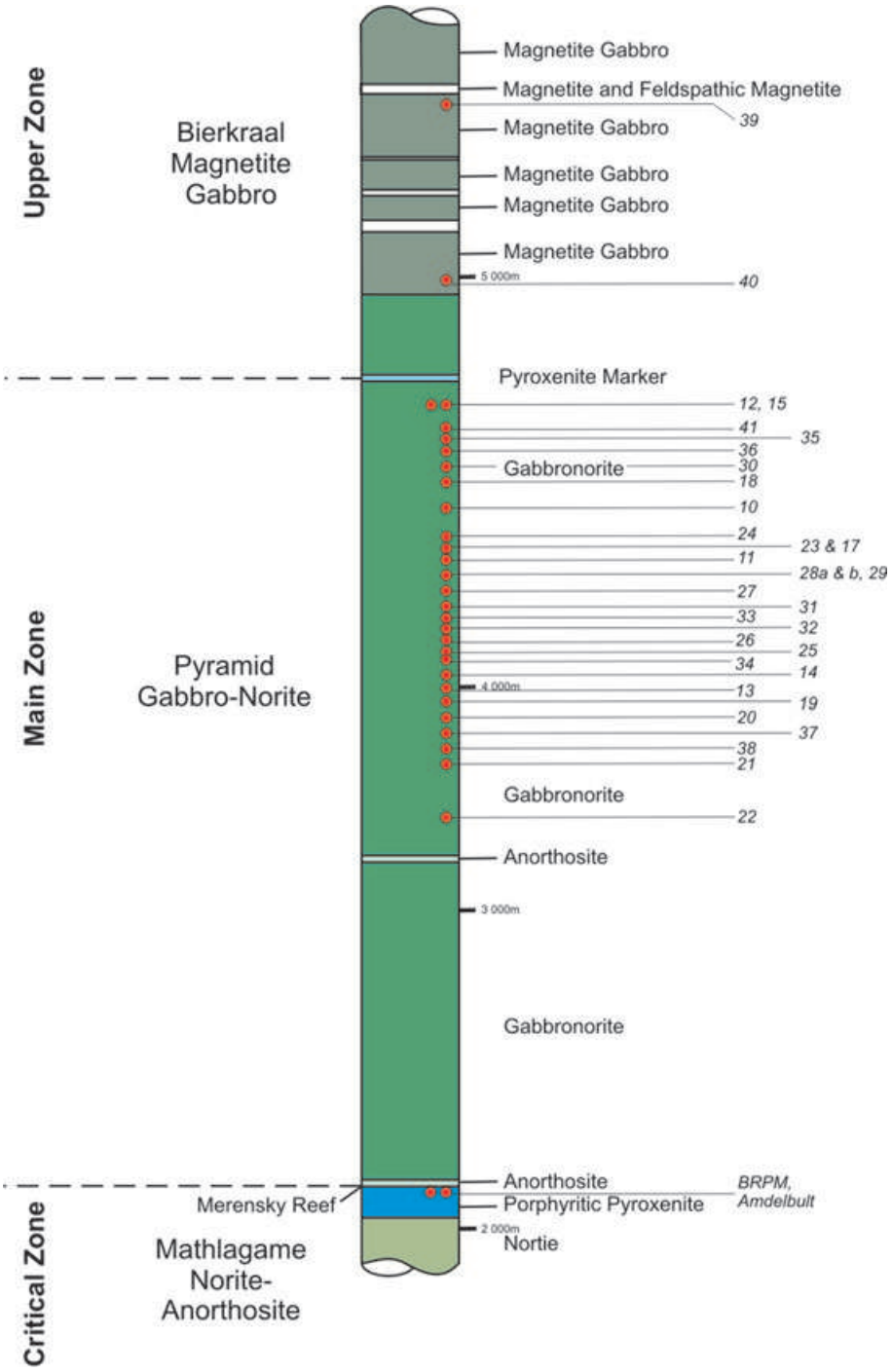

Figure 2. Lithostratigraphic column of the Rustenburg Layered Suite in the Western Bushveld with site locations (modified after SACS 1980). Stratigraphic positions are based on Hattingh (1983) site locations.

2.4 Upper Zone

Palaeomagnetic drill locations were extremely limited, with only eight sampling sites being obtained (Fig. 7a), two from the Western Lobe and the remaining six from the Eastern Lobe, and located to riverbeds and road cuttings.

2.5 Northern Lobe Main Zone

The Northern Lobe is exposed over a 110 km in length, starting ∼35 km to the southwest of Mokopane and extending north. In total, 27 sites were obtained (Fig. 8): 23 from the Main Zone located in the vicinity of Mokopane and four from the Upper Zone near Villa Nora.

3 THERMOMAGNETIC AND PETROGRAPHIC ANALYSIS

Thermomagnetic analysis (TMA) and petrographic analysis (reflected and transmitted light microscopy) were undertaken to identify the opaque mineralogy and to determine the potential carrier

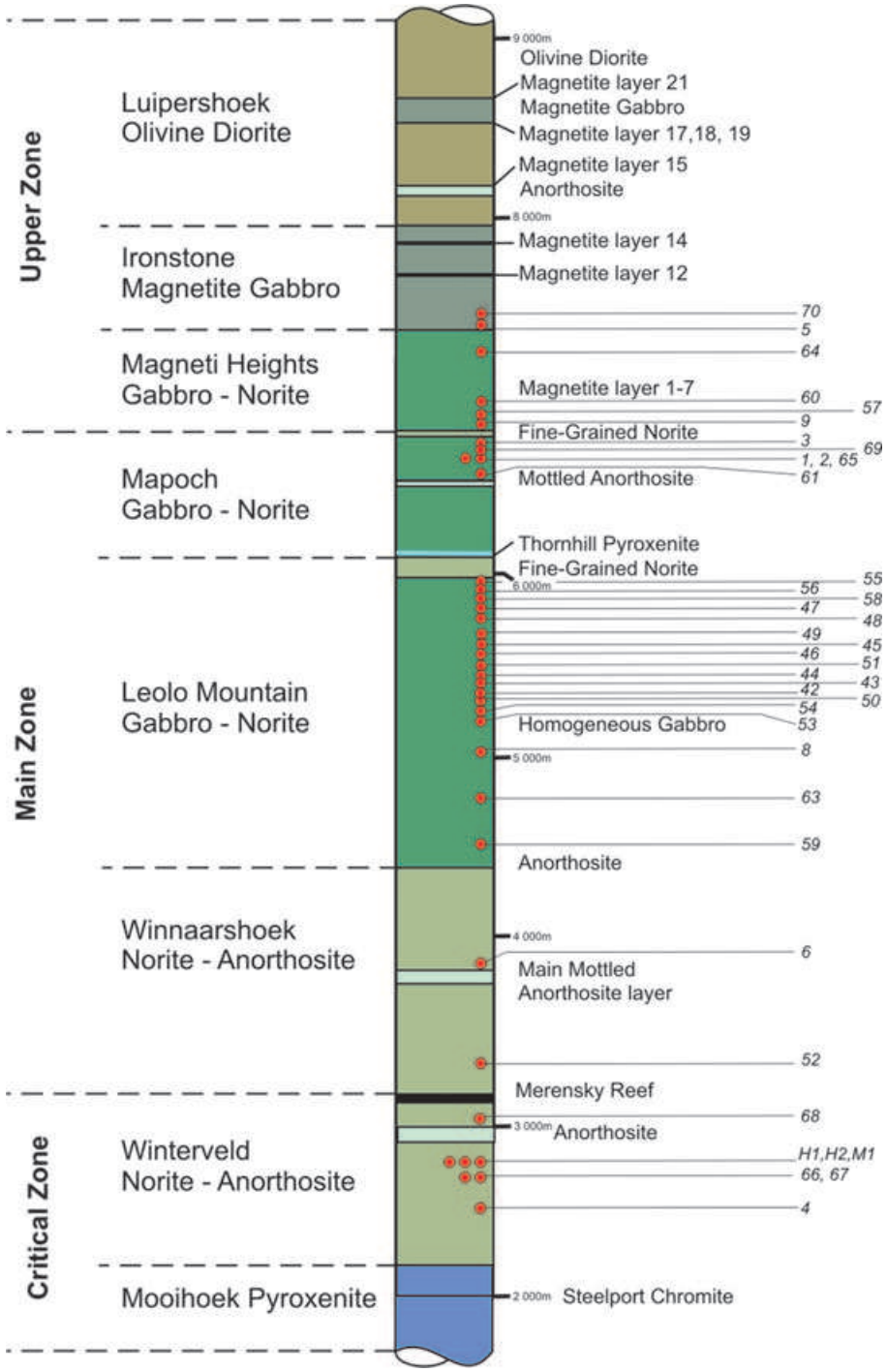

Figure 3. Lithostratigraphic column of the Rustenburg Layered Suite in the Eastern Bushveld with site locations (modified after SACS 1980). Stratigraphic positions are based on Hattingh (1983) site locations.

of magnetization (Section 4). TMA (Curie temperature determinations) was conducted on a Translation Bridge built *in-house* at the Geological Survey in Trondheim.

3.1 Main Zone, Western Lobe

Curie-curves are almost reversible with Curie temperatures at around 580°C, implying the presence of magnetite (Fig. 9a), and samples throughout the western Main Zone contained a similar mineralogy. Magnetite is the dominant mineral and occurred as lamellae or needles in both plagioclase and pyroxene, and in rare occasions as discrete grains. A number of large needles of magnetite were identified by reflected light microscopy (Fig. 9b). However, the smaller lamellae could not be positively identified as magnetite due to their small size. Previous petrographic analyses of Main Zone rocks have also identified the occurrence of magnetite as needles in both plagioclase (Groeneveld 1970; Scharlau 1972; Hattingh 1983) and pyroxene (Scharlau 1972; Hattingh 1983). On average, the needles were 4.5 μm long and 1.5 μm wide for pyroxene and 10 μm

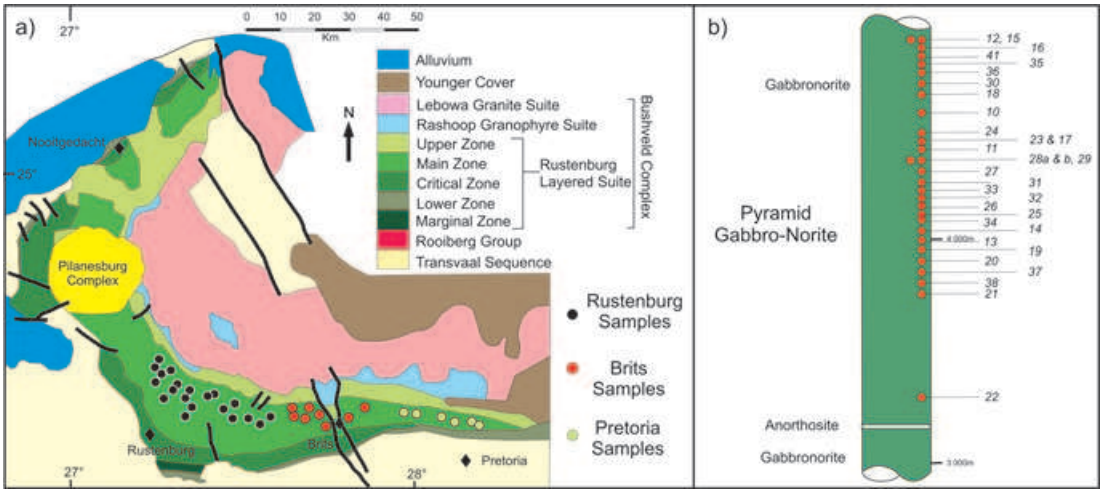

Figure 4. (a) Simplified geological map of the Western Bushveld Complex, indicating the locations of sites. (b) Simplified stratigraphic column of the western Main Zone, indicating locations of sites (modified after SACS 1980).

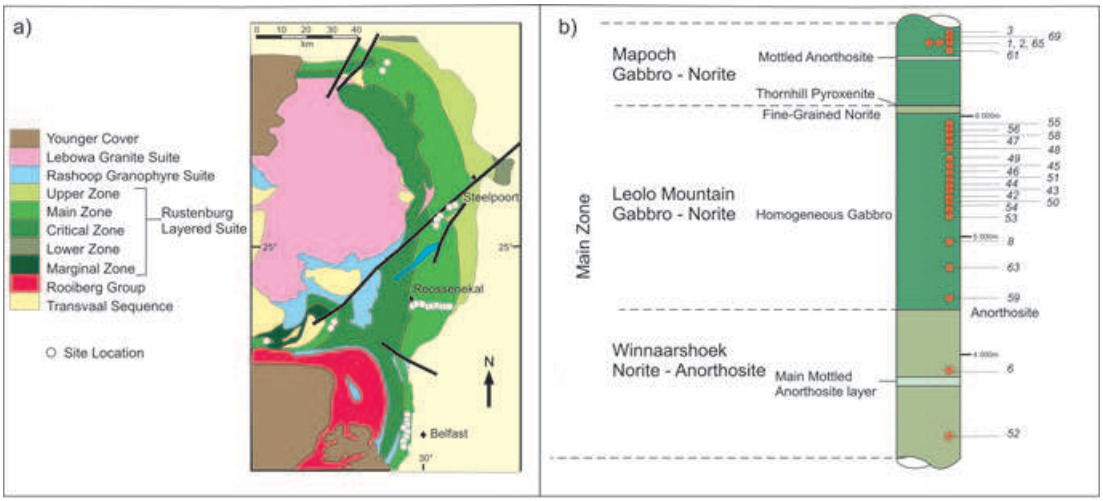

Figure 5. (a) Simplified geological map of the Eastern Bushveld Complex, indicating the locations of sites. (b) Simplified stratigraphic column of the eastern Main Zone, indicating locations of sites (modified after SACS 1980).

long and 1 μm wide for plagioclase. Based on Curie temperatures of ~580 °C it was concluded that the lamellae observed by transmitted light microscopy (Figs 9c and d) are magnetite. Minor discrete ilmenite and pyrrhotite grains were also found.

3.2 Main Zone, Eastern Lobe

Typical response to TMA is shown in Fig. 10(a) in which curves are almost reversible, except for a small increase in saturation magnetization upon cooling. Samples indicate a Curie temperature of ~580°C. Reflected light microscopy revealed a minor number of large lamellae of magnetite occurring in both pyroxene and plagioclase (Fig. 10b). In transmitted light, it was discovered that smaller lamellae (Figs 10c and d) are more abundant but due to their small size, they could not be positively identified as magnetite. However, based on TMA and the appearance of larger lamellae, we suggest that the small lamellae are most likely magnetite. Subordinate discrete ilmenite and pyrrhotite grains were also identified.

3.3 Critical Zone

TMA reveals Curie temperatures of ~580°C. Petrographic analysis failed to identify magnetite in thin section. Magnetite might occur as needles or lamellae in both plagioclase and pyroxene; however, grains were too small to identify. Due to TMA analysis that revealed a Curie temperature of ~580 °C, it is assumed that the lamellae are magnetite as identified in all other zones.

3.4 Upper Zone

Once again, TMA indicates that samples have a Curie temperature of ~580°C. Petrographic analysis (Fig. 11) revealed the presence of discrete magnetite grains occurring in a variety of sizes from as small as 9 μm up to large 90 μm. The occurrence of magnetite as exsolution lamellae in pyroxene and plagioclase is observed to a minor degree, but is not as abundant as is observed in the Main Zone. Ilmenite is also present as large discrete grains. The susceptibility of these rocks is quite high with values consistent with previous studies in the Upper Zone of the Northern Lobe (Ashwal *et al.* 2005).

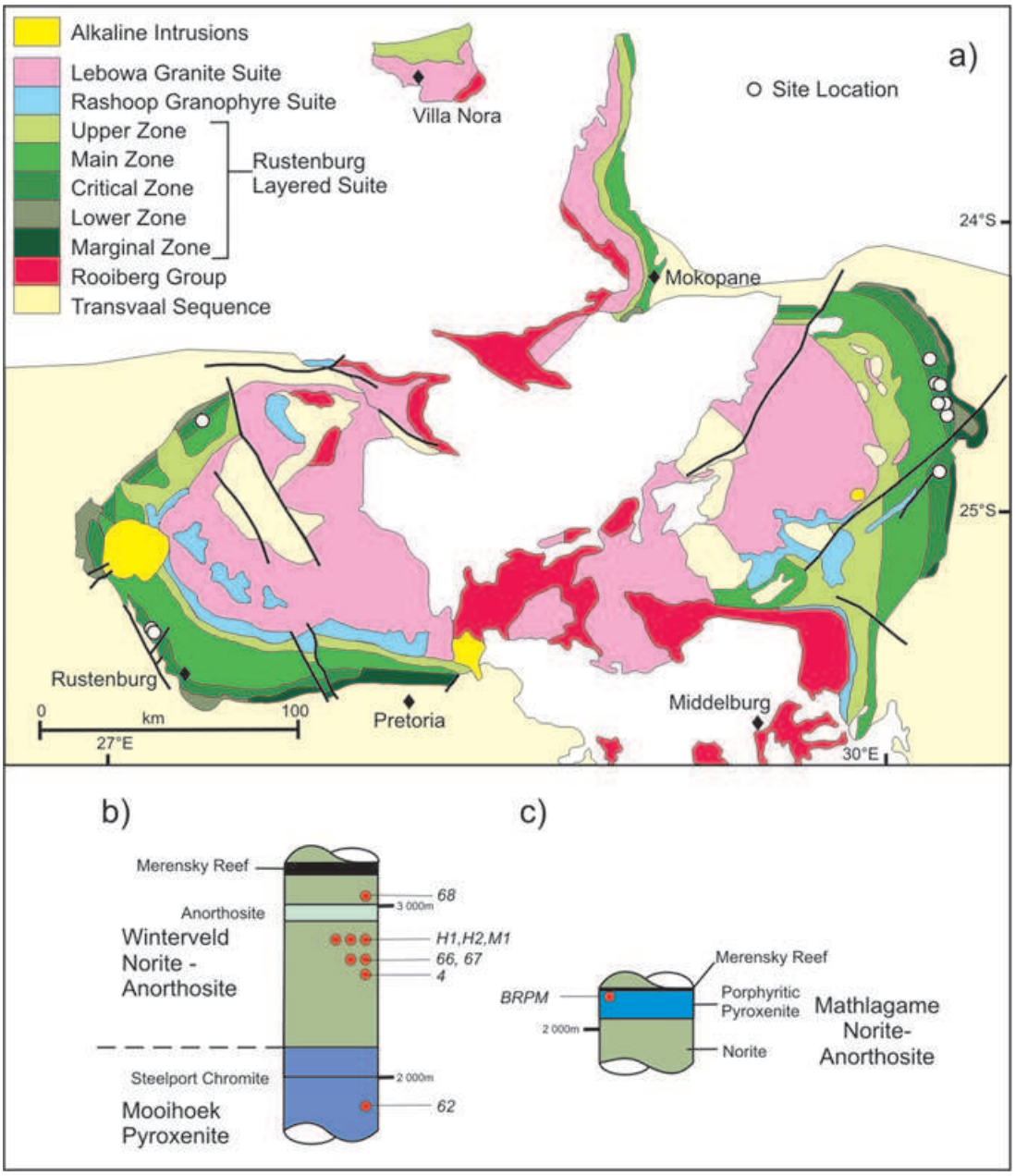

Figure 6. (a) Simplified geological map of the Bushveld Complex, indicating the locations of Critical Zone sites. Simplified stratigraphic column of the Critical Zone for both the Eastern Lobe (b) and Western Lobe (c) with site locations. H1 and H2 are from Hackney Mine, whereas M1 is from Modikwa mine.

3.5 Northern Lobe Main Zone

TMA reveal almost reversible Curie curves with Curie temperature of ∼580°C. Polished thin sections studied revealed the presence of various sulphides (pyrrhotite being the majority) and ilmenite (Fig. 12). Magnetite was identified as both discrete grains and as needles within plagioclase and pyroxene crystals.

4 PALAEOMAGNETIC RESULTS AND FIELD STABILITY TESTS

The natural remanent magnetization (NRM) was measured on a JR6A spinner magnetometer, whilst the bulk susceptibility was measured on a Bartington MS2 system (Table 2). Most sites have high Koenigsberger ratios [Q = remanent magnetization/(susceptibility × induced magnetization); local geomagnetic field ∼30.000 nT), on average 41, and demonstrate that remanence is especially important to incorporate in magnetic modelling. Because magnetic modelling is conducted on rocks in their present day orientation (i.e. not corrected for folding), the values in Table 2 are the values that should be used to incorporate NRM in magnetic modelling of the current day magnetic response.

Stability of the NRM was tested by thermal demagnetization using a MM-TD-60 furnace and alternating field (AF) demagnetization with the use of a two-axis tumbler demagnetizer. Demagnetization data were analysed in orthogonal vector plots (Zijderveld diagrams) and characteristic remanence components were calculated by means of principle component analysis (Kirschvink 1980) implemented in the Super-IAPD software (Torsvik *et al.* 2000). Low

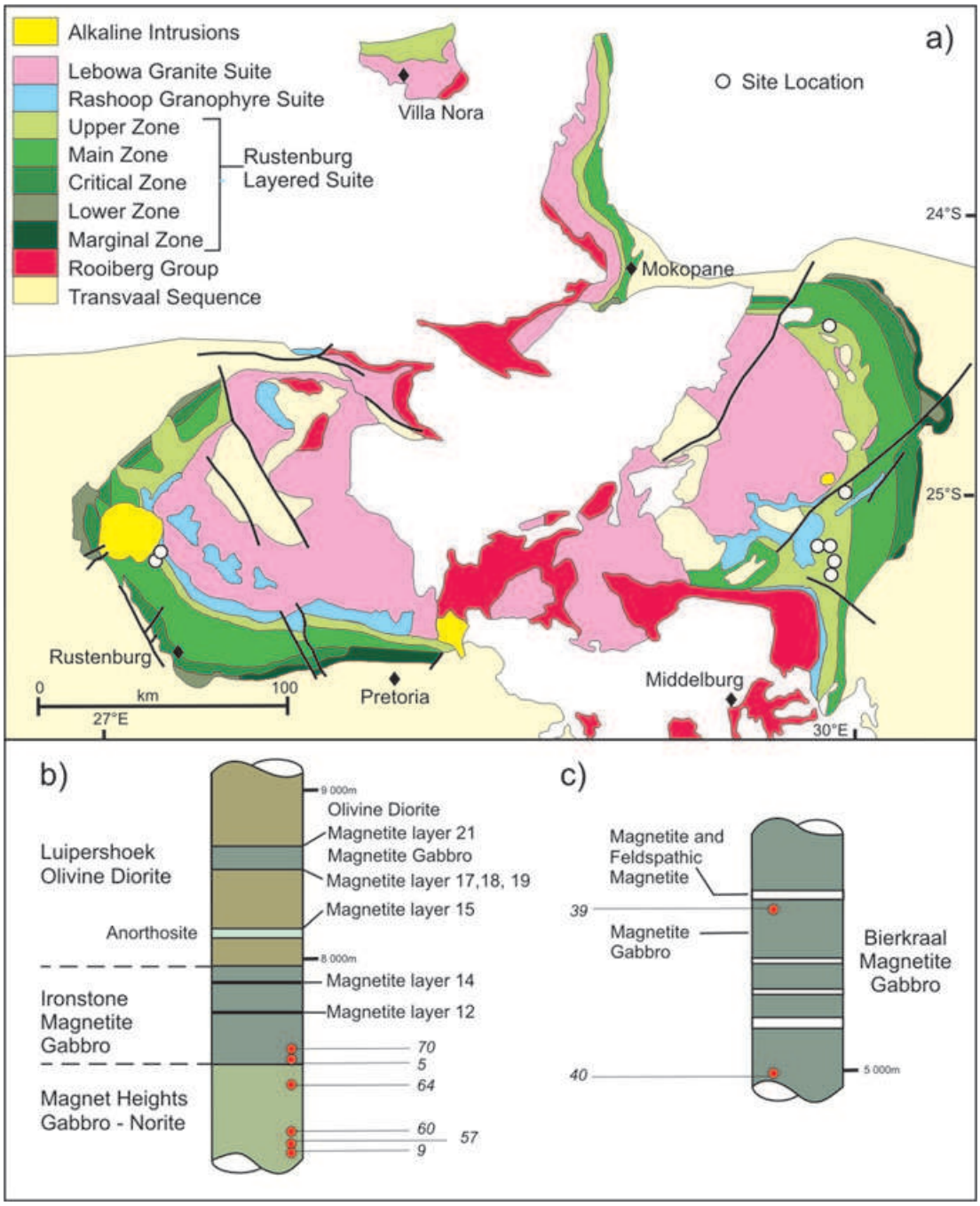

Figure 7. (a) Simplified geological map of the Bushveld Complex, indicating the locations of sites. Simplified stratigraphic column of the Upper Zone indicating locations of sites for the Eastern Lobe (b) and Western Lobe (c).

unblocking/coercivity components identified during demagnetization experiments are not listed in Tables 3–7.

4.1 Main Zone, Western Lobe

Most samples contain two components of magnetization (Fig. 13): a low coercivity or low unblocking (LB) component and a high coercivity or unblocking (HB) component. In most cases LB components are poorly defined; they are randomly orientated and typically demagnetized below 300–400°C or 30 mT. With the removal of LB components, well-defined HB components were identified at ∼560–580°C or above 50 mT. Although the maximum AF demagnetization field of 95 mT did not completely demagnetize all samples, NRM intensities were reduced to 35–19%, and showed the same behaviour as thermal demagnetization, with clear decay towards the origin of the vector plots. HB components show good clustering, and produce well-grouped results within sites (Fig. 14; Table 3). Upon completion of demagnetization, the grouping in NRM directions (based on geographical location of sites, that is Rustenburg, Brits and Pretoria) formed tighter clusters. Sites located near Pretoria produced HB components with steep positive

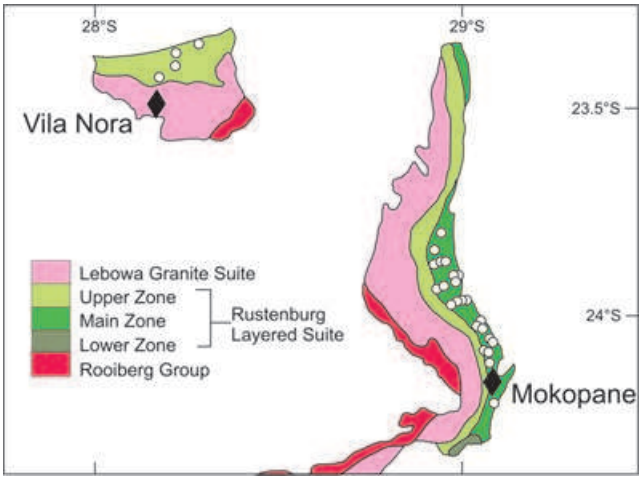

Figure 8. Simplified geological map of the Northern Lobe of the Bushveld Complex, indicating the locations of samples.

inclination and southern to southwest declination (Figs 13a and d and 14). Sites in the vicinity of Brits have steep positive inclinations with northeast declinations (Figs 13b and e and 14) whilst sites located around Rustenburg have steep positive inclinations with northwest declinations.

To test if HB components have a pre-, syn- or post-fold origin, a classical fold test was undertaken (McElhinny 1964). Stepwise bedding corrections were applied to all HB components until the layers were restored to a horizontal attitude. To test if dual-polarity site-means share a common mean, the reversal tests of McFadden & Lowes (1981) and McFadden & McElhinny (1990) were implemented. Although the polarity of the Earth's magnetic field is unknown at 2054 Ga, we refer to steep positive inclinations with mostly northerly declinations as REVERSE polarity whilst negative inclinations with southerly declinations are denoted as NORMAL polarity.

Rocks from the Western Lobe form an arc from Pretoria through to the Pilanesburg Complex, dipping towards the centre of the complex at angles of between 10° and 25° (dips and strikes listed in Table 3). Upon stepwise unfolding, a uniform increase in statistical precision parameter κ was observed from 58.5 to 169.3 (Fig. 14c). This can be seen noticeably in graphical representation by the increase in directional clustering (Fig. 14b), and the classical fold test produced a positive fold test at the 95% confidence level. All site-mean directions possessed positive inclinations (reverse polarity) except site 28b. The reversal test (McFadden & Lowes 1981) shows that the sites shared a common mean at 95% confidence level. The McFadden & McElhinny (1990) reversal test could not be implemented due to only one site with opposite polarity.

4.2 Main Zone, Eastern Lobe

Typical behaviour upon demagnetization is shown in Fig. 15. The majority of samples obtained from road cuttings were composed of two components of magnetization, LB and HB. On the other

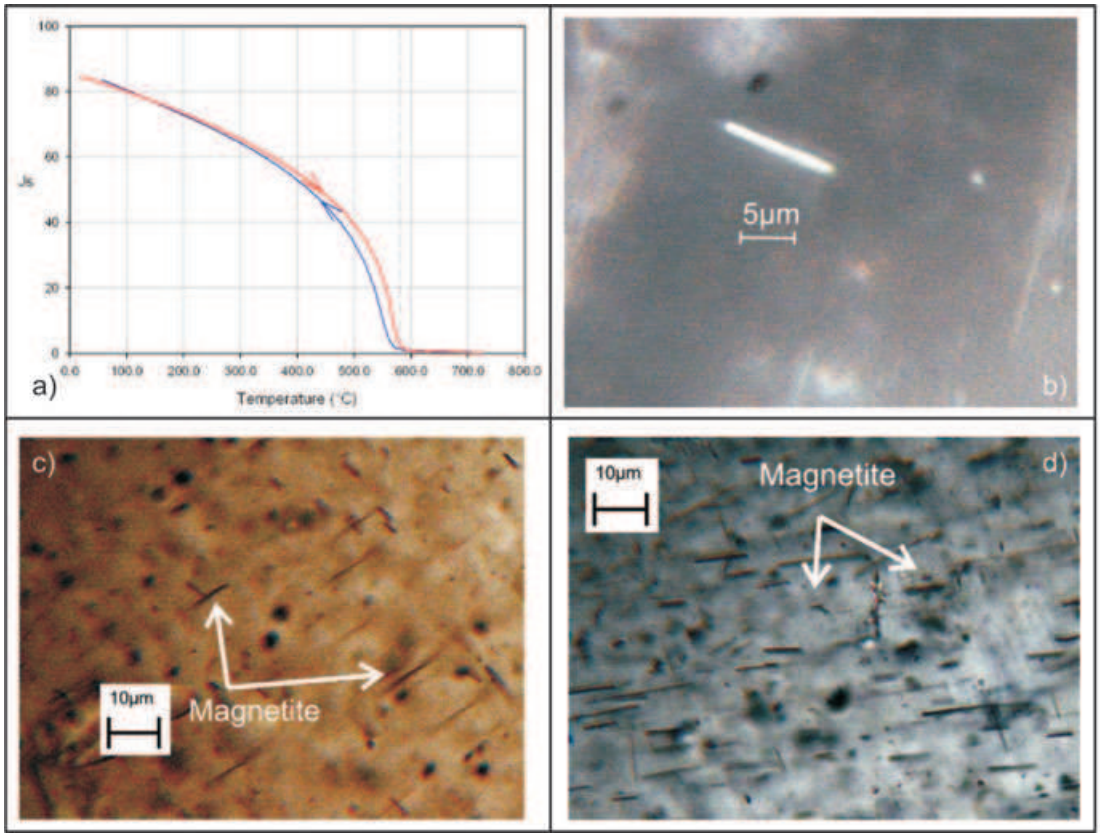

Figure 9. (a) Typical TMA response from site 12 occurring in the Main Zone of the Western Lobe. Red line and arrow indicate heating phase whereas blue line and arrow indicate cooling phase. Curie temperature for magnetite at ≈580°C observed (dashed line). (b) Needle of magnetite occurring in a plagioclase grain from site 29, reflected light. (c) Needles or lamellae of magnetite occurring in a pyroxene from site 24, transmitted light. (d) Needle of magnetite occurring in a plagioclase from site 37, transmitted light.

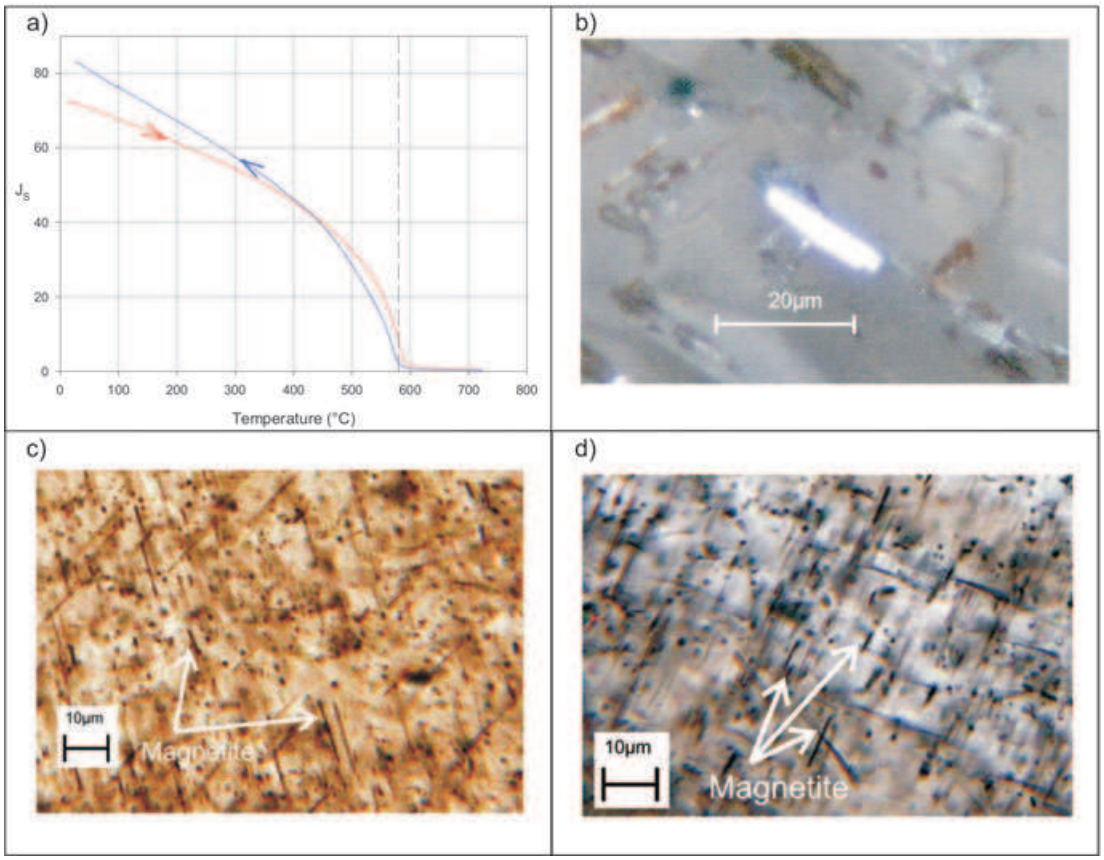

Figure 10. (a) Typical TMA response from Eastern Main Zone sites, this example is from site 52. Red line and arrow indicate heating phase whereas blue line and arrow indicates cooling phase. Curie temperature for magnetite at ≈580 °C observed (dashed line). The observed increase in saturation magnetization during cooling implies the possible production of more magnetite. (b) A "large" magnetite needle occurring in plagioclase grain from site 70, reflected light. (c) Magnetite occurring as needles in pyroxene from site 8, transmitted light. (d) Magnetite occurring as needles in plagioclase grain from site 44, transmitted light.

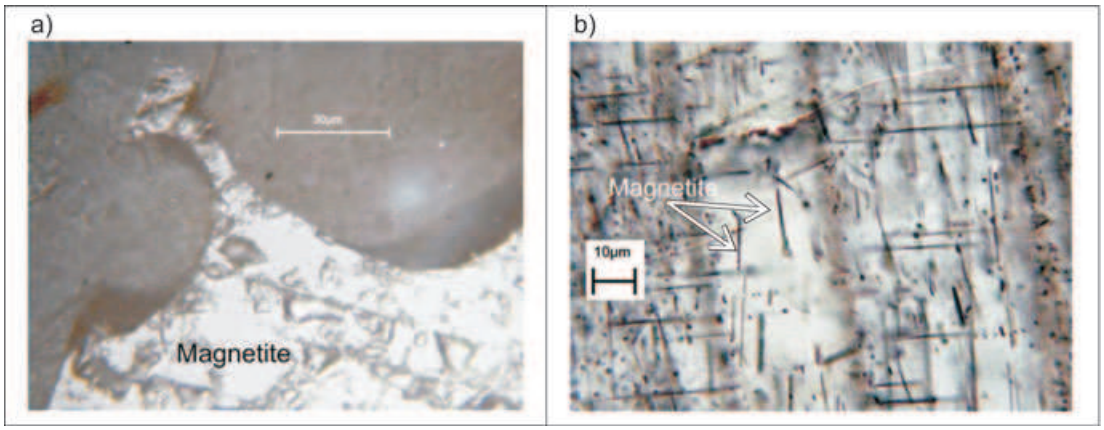

Figure 11. (a) Thin section analysis revealed the occurrence of a magnetite in a variety of sizes, thin section obtained form site 57. (b) Petrographic analysis of plagioclase from the Upper Zone revealed lamellae of magnetite (transmitted light), thin section from site 39.

hand, samples from dimension stone quarries (Figs 15a and d) show almost univectorial demagnetization behaviour and in rare instances where LB components were present they were often removed after only two or three demagnetization steps. LB components are present but they are randomly scattered both within and between sites. These overprints are more persistent then those present in the Western Lobe, and are typically removed at around 500°C or 30–40 mT. They show no correlation with any known remanence direction for the region or that of the present-day magnetic field. Removal of LB components isolates well-defined HB components that are identified above 550°C and 50 mT. Both thermal and AF demagnetization yielded similar directional results. As in the Western Lobe, a few sites were not completely demagnetized by AF demagnetization and required additional thermal demagnetization.

HB components (Table 4) show extremely good grouping within sites, with α_{95} often $<4°$ (Fig. 16), and the resulting mean directions

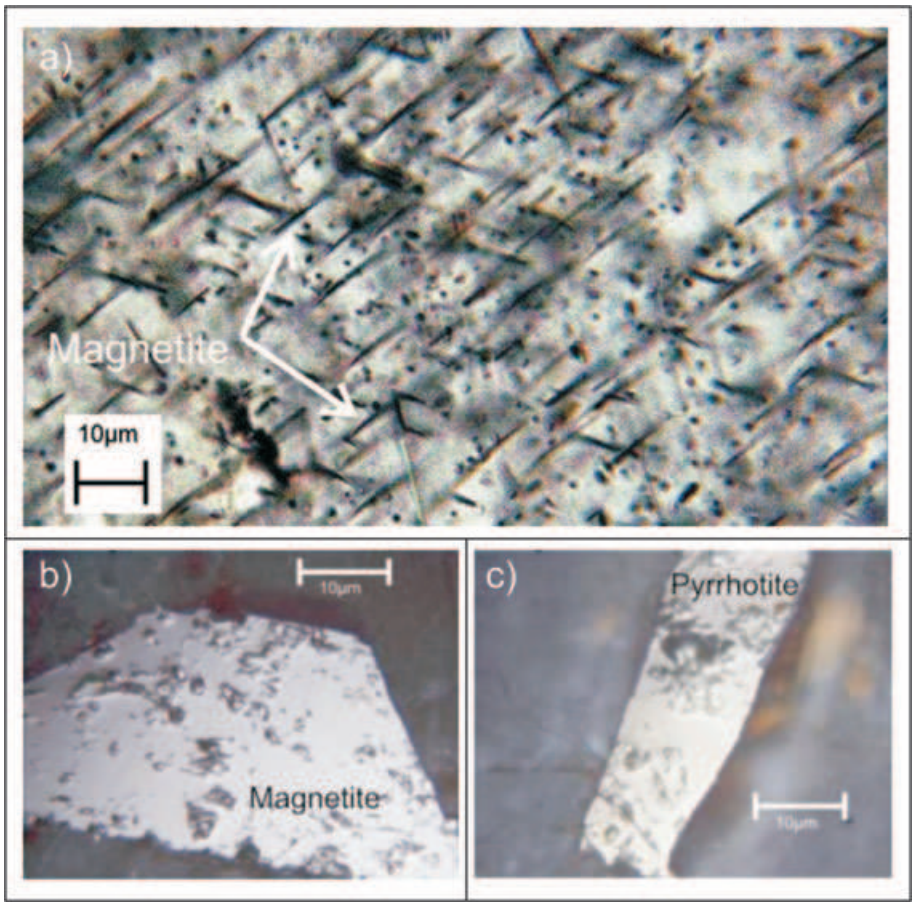

Figure 12. (a) Polished then section from site 15 in the Main Zone of the Northern Lobe indicating magnetite lamellae occurring in plagioclase, transmitted light. Polished thin section images form reflected light indicating a large grain of magnetite (b) from site 4 and a pyrrhotite grain (c) from site 24.

for sites show a remarkable increase in clustering compared with the original NRM directions. HB directions for sites show both positive and negative inclination, with the majority of the sites possessing HB components with steep positive inclinations and northeast declinations, whereas the remaining six sites have steep negative inclinations with southwest declinations.

Rocks from the Eastern Lobe outcrop in a crude "hook" shape, dipping towards the centre of the complex at angles of between 10 and 15°. This "hook" shape is produced initially from Belfast to Steelpoort, where rocks have a north-south trend and dip towards the west at angles of between 10 and 15°. Moving from Steelpoort further north, rocks curve towards the west with approximately NW strikes, and dip inwards in a SW direction. Upon unfolding a uniform increase in statistical precision parameter κ was observed from 47.7 to 83.2 (Fig. 16c). The resulting increase in κ produces a positive fold test at the 95% confidence level. Samples from the eastern Main Zone possess dual polarity directions and the samples share a common mean at 95% confidence. The reversal test by McFadden & McElhinny (1990) also indicated a positive reversal test with a "C" classification, $\gamma_{\text{observed}} = 5.4$ and $\gamma_{\text{crit}} = 10.4$.

4.3 Critical Zone

Samples from BRPM2 and M2 (Modikwa mine) were unstable during demagnetization and results were rejected from further analysis. Remaining samples behaved exceptionally well to both thermal and AF demagnetization, and two magnetization components have been readily identified (Fig. 17). LB components are present in most samples, but they are mostly scattered at site-level and typically removed at around 500°C or 30–40 mT. Their directions are not related to any significant geological meaning and are not considered further.

With the removal of LB components, dual-polarity components were isolated above 550°C or 50 mT. These HB components show reasonable grouping within-site (α_{95} around 6°), and mean site directions plot with a SSW declination and steep negative inclination or antipolar to this (NNE declination and steep positive inclination; Fig. 18; Table 5).

Rocks of the Critical Zone all dip towards the centre of the Bushveld Complex, with varying dip angles of between 10° and 18°. Upon unfolding, site-mean directions showed a minor increase in grouping (Fig. 18) and precision parameter κ increased from 42.4 to 67.5 associated with a slight decrease of α_{95} from 8.1 to 6.8; this minor improvement was not sufficient to produce a positive fold test of McElhinny (1964). The samples share a common mean at 95% confidence (McFadden & Lowes 1981). The McFadden & McElhinny (1990) reversal test indicated a positive reversal test with a "C" classification, $\gamma_{\text{observed}} = 5.7$ and $\gamma_{\text{crit}} = 16.1$.

4.4 Upper Zone

Fig. 19 includes a selection of orthogonal plots. Typically two components of magnetization were identified as LB and HB. In some cases, three components or perhaps strongly overlapping

Table 2. Palaeomagnetic sampling locations (GPS Lat. = latitude; Long = longitude for surface sites), mean NRM directions and intensity, bulk susceptibility (suscept.) and Q ratio (calculated with a local geomagnetic field of 30.000 nT). And α_{95} = 95 percent confidence circle around mean direction, N = number of samples, $\pm 1\sigma$ error.

Site	Lat. (S)	Long. (E)	NRM declination	NRM inclination	α_{95}	N	NRM intensity (A/M)	±(mA/m)	Suscept. ($\times 10^{-6}$ SI)	± ($\times 10^{-6}$)	Q ratio
Main Zone, Western Lobe (30 sites)											
10	25°37.62	28°12.89	46.8	88.8	2.3	9	1.69	104.1	1278.0	71.5	55
11	25°36.43	28°03.03	248.4	77.2	6.8	9	0.54	151.7	787.4	206.1	28
12	25°34.62	27°40.05	14.8	87.1	1.5	9	8.38	555.6	2705.6	285.8	130
13	25°36.58	27°39.43	5.2	63.7	9.8	9	1.54	175.6	1127.7	152.0	57
14	25°36.54	27°37.28	10.7	70.9	2.8	9	1.54	58.7	912.8	41.3	71
15	27°37.28	27°38.26	39.1	81.6	2.6	9	8.38	1568.7	4947.5	1182.7	71
16	25°34.79	27°38.16	20.5	82.9	2.2	9	5.32	1017.3	3974.4	945.5	56
17	25°36.43	28°04.55	47.0	89.2	1.4	9	0.66	74.1	661.4	54.8	42
18	25°37.06	28°11.97	124.2	85.3	2	9	0.42	33.7	520.8	30.5	34
19	25°36.28	27°41.66	90.0	68.5	18.9	9	0.68	130.3	683.7	67.8	42
20	25°37.06	27°34.81	36.2	64.6	7.1	9	0.79	114.3	577.6	18.2	58
21	25°35.99	27°52.45	27.4	72	3.8	9	0.39	32.1	525.1	51.0	31
22	25°37.15	27°48.04	35.7	62.2	2.5	9	1.50	87.2	1031.7	133.9	61
23	25°30.86	27°18.44	339.0	75.4	1.3	9	1.55	128.6	904.4	101.1	72
24	25°31.17	27°19.12	29.9	66.1	7.6	9	2.37	446.1	919.7	60.6	108
25	25°32.57	27°20.06	334.6	72.5	3.8	9	1.04	78.7	877.2	103.9	50
26	25°32.86	27°19.91	324.3	73.1	1.2	9	1.75	89.2	899.5	92.0	82
27	25°32.78	27°21.26	256.9	83	22.1	9	2.43	404.7	551.5	14.9	185
28	25°32.15	27°20.55	315.0	70.1	25.9	9	1.17	505.5	491.0	82.0	100
29	25°32.00	27°20.36	335.0	78.4	6.9	9	0.96	59.2	492.3	47.7	81
30	25°31.52	27°19.71	323.0	74.8	9.1	9	1.87	176.5	742.8	97.1	105
31	25°33.03	27°21.97	327.0	75	1.5	9	1.13	72.8	610.6	39.4	77
32	25°33.49	27°22.32	327.0	79.9	1.2	9	1.62	145.5	702.3	91.0	97
33	25°34.01	27°22.26	338.2	75.4	2.9	9	3.62	242.3	1194.6	144.8	127
34	25°34.51	27°23.37	342.7	75.9	2.8	9	1.25	51.6	869.3	54.5	60
35	25°32.88	27°25.74	333.2	70.4	2.6	11	2.41	319.5	1553.4	275.9	65
36	25°31.82	27°22.05	184.2	−18.3	4	11	0.90	62.0	2376.5	184.2	16
37	25°36.42	27°30.06	348.1	69.9	5.3	9	1.33	133.4	799.5	39.1	70
38	25°36.06	27°32.49	41.3	68.5	8.8	5	1.14	68.5	595.8	33.0	80
41	25°32.86	27°26.04	4.1	72.3	2.2	9	1.46	123.5	1312.2	163.5	47
Main Zone, Eastern Lobe (26 sites)											
1	24°52.28	30°02.65	220.0	−66.6	4.5	9	0.21	68.72	691.95	53.83	13
2a	24°52.36	30°02.66	220.5	−59.4	4.5	7	0.16	79.22	391.00	108.10	17
2b	24°52.36	30°02.66	209.2	−56.3	2.8	7	0.19	85.21	483.00	95.21	17
3	24°57.25	29°57.93	201.2	−47.7	6.4	14	0.29	172.79	1511.71	488.83	8
8	25°13.50	30°00.46	36.2	61.9	2.8	8	0.61	32.54	784.38	43.85	33
42	25°35.84	29°55.53	35.9	64.8	2.4	9	16.89	561.77	4979.83	317.16	142
43	25°35.88	29°55.32	30.8	61.4	2.4	10	6.95	677.46	4027.01	234.05	72
44	25°36.03	29°55.31	48.5	61.4	2.8	8	7.56	569.66	4260.68	304.61	74
45	25°41.01	29°55.04	30.2	67.9	1.6	9	17.08	638.88	3206.57	165.34	223
46	25°40.92	29°55.01	35.8	62.5	1.5	10	15.39	1596.73	3394.95	129.94	190
47	25°40.82	29°54.73	39.5	62.7	1.1	9	25.31	762.31	3936.42	183.84	269
48	25°41.34	29°54.84	35.7	64.1	1.4	7	28.87	729.23	2744.13	159.28	441
49	25°41.16	29°55.04	32.8	66.7	0.9	8	16.28	517.97	3231.45	198.12	211
50	25°36.98	29°55.58	31.1	57.2	2.7	9	18.77	2071.53	5812.99	445.83	135
51	25°36.75	29°55.23	46.4	59.3	1.9	9	10.73	1039.60	5724.38	849.27	79
52	25°20.31	29°22.77	14.3	33.9	8.7	4	3.93	1323.82	704.78	120.73	234
53	25°15.85	29°37.57	14.6	62.7	7.1	8	2.14	622.14	1810.91	604.03	50
54	25°15.94	29°37.48	1.2	66.2	2.4	9	1.54	153.01	3520.69	332.47	18
55	25°12.01	29°55.86	45.5	60.8	3.3	8	6.49	2651.42	7503.73	362.31	36
56	25°11.87	29°56.08	32.9	57.7	7.5	5	0.18	43.17	495.27	56.31	15
58	25°12.08	29°58.00	45.5	60.8	3.3	8	3.16	1211.59	6260.26	718.48	21
59	25°13.17	30°00.89	358.2	75.1	4.4	6	10.63	3765.73	8947.39	2760.22	50
61	24°57.68	29°57.39	203.0	−62.3	5.0	8	0.67	105.26	1271.74	290.22	22
63	24°20.12	29°45.9	19.5	54.8	3.8	9	2.99	613.04	16490.38	3788.26	8
65	24°22.61	29°46.88	20.8	27.9	3.6	8	0.02	2.51	691.97	114.05	1
69	24°56.31	29°53.17	218.2	−71.1	4.0	8	0.31	85.05	1262.31	607.92	10

Table 2. (*Continued.*)

Site	Lat. (S)	Long. (E)	NRM declination	NRM inclination	α_{95}	N	NRM intensity (A/M)	±(mA/m)	Suscept. ($\times 10^{-6}$ SI)	± ($\times 10^{-6}$)	Q ratio
Critical Zone (9 sites)											
4	24°53.21	30°07.63	50.7	24.4	54.4	13	0.3	0.2	114.8	35.0	0.4
66	24°38.04	30°8.32	178.4	−51.9	10.6	8	15.5	5.8	230.6	81.6	0.8
67	24°38.42	30°08.04	175.1	−35.6	18.3	9	14.9	5.7	274.9	60.3	0.9
68	24°24.07	30°00.83	333.2	32.6	14.5	9	15.3	4.8	275.2	166.9	0.9
M	Modikwa mine		224.1	−73.5	2.8	11	467.3	41.3	379.1	29.4	1.3
B1	Amandelbuilt mine		147.9	23.9	63.1	9	462.7	255.0	1016.8	556.0	3.4
B2	Amandelbuilt mine		354.2	60.9	55	10	8.4	6.8	518.2	152.6	1.7
H2	Hackney mine		67.5	11.8	3.4	10	96.5	25.8	385.7	72.7	1.3
H1	Hackney mine		166.2	−41.5	9.4	6	40.4	6.3	245.2	27.0	0.8
Upper Zone (8 sites)											
5	25°06.53	29°53.11	212.0	−62.0	6.7	11	4.8	1293.9	750.0	118.2	24
9	25°22.26	29°51.28	6.5	52.3	23.2	9	1.7	428.6	16191.9	1939.0	0.4
39	25°20.85	27°12.43	155.6	−77.6	28.5	13	5.1	647.3	50094.2	23916.0	0.4
40	25°22.55	27°12.43	130.1	−27.4	13.5	13	0.3	182.9	652.9	190.7	1.9
57	25°22.89	29°50.31	319.0	−21.2	16.9	13	28.9	19735.5	30083.0	7870.4	3.6
60	25°11.54	29°53.78	198.4	−6.4	29.5	9	30.7	13113.7	21980.1	10500.7	5.3
64	24°24.92	29°47.35	175.4	−60.9	41.0	9	3.5	345.5	7220.9	1381.3	1.8
70	25°10.06	29°50.08	342.0	−76.7	12.5	9	42.2	3886.15	N/A	N/A	N/A
Northern Lobe, Main Zone (27 sites)											
1	24°13.64	29°02.07	42.3	46.7	6.5	9	492.78	29.03	1114.3	142.8	19
2	24°09.55	28°58.07	247.9	78.6	59.6	9	1192.08	663.66	791.2	80.3	63
3	24°09.01	28°57.78	67.4	72.3	35.4	9	860.39	192.62	633.2	33.2	57
4	24°09.21	28°57.87	11.4	52.6	7.1	9	1530.70	662.59	818.3	239.9	78
5	28°57.87	28°58.64	9.3	52.1	39.5	8	4744.56	1441.80	1071.2	183.8	186
6	24°08.42	28°58.53	21	54.4	10.6	19	187.26	88.94	286.0	58.4	27
7	24°02.09	28°54.09	0.4	32.5	32.6	9	8.29	4.91	285.0	23.6	1
8	24°00.31	28°52.33	208.8	−48.1	17	9	14.57	4.45	545.0	33.7	1
9	24°01.09	28°51.75	323.7	51.1	5.7	10	5716.24	700.13	6986.5	2366.5	34
10	24°02.05	28°54.14	51.2	67.2	12.8	9	2319.47	1292.81	1752.3	1198.5	55
11	24°02.45	28°54.14	45	64	18	9	11.43	4.38	280.2	20.2	2
12	24°02.75	28°54.14	23.7	23.6	9.2	8	113.05	38.14	690.5	70.0	7
13	24°03.95	28°58.09	9.4	48.2	11.5	9	1094.96	527.80	526.9	50.9	87
14	24°03.75	28°58.09	21.9	63.4	36.9	9	110.14	15.68	838.5	142.8	6
15	24°03.85	28°58.18	183.3	−49	10.2	9	164.87	42.65	1878.9	648.0	4
16	23°29.83	28°10.23	281.6	70.3	40.1	9	1873.99	1082.47	1119.1	598.5	70
17	23°27.27	28°09.92	123.4	87.4	29.3	7	268.46	153.55	76.8	17.0	146
18	23°26.00	28°12.00	16.6	55.6	45.9	10	160.51	39.14	304.0	96.3	22
19	23°31.00	28°07.05	300.6	32.7	57	6	14620.15	1655.62	1843.6	778.6	332
20	23°56.83	28°50.52	114.4	77.6	24.4	10	763.43	310.62	301.4	129.4	106
21	23°56.72	28°50.64	56.3	61.8	17.6	11	817.03	354.41	564.6	143.3	61
22	23°56.09	28°50.42	41.2	62.7	3.5	9	1272.26	403.90	245.1	70.1	217
23	23°55.14	28°49.25	73.9	61	11.7	8	3126.01	434.20	2096.4	344.5	62
24	23°52.81	28°49.35	161	35.8	37.1	7	589.40	94.29	822.1	178.1	30
25	23°59.31	28°53.89	34.9	39.2	53.1	6	5.78	2.14	260.1	60.4	1
26	23°59.21	28°53.93	9.1	28.2	48.7	5	7.52	1.75	301.4	60.7	1
27	23°59.03	28°54.25	52.1	39.2	41	8	52.81	12.53	574.0	17.9	4

blocking/coercivity spectra of LB and HB components are recognized. In general LB components are mostly scattered at site level but *in situ* LB components from two sites plot close to the present magnetic field in South Africa and probably represent a recent viscous overprint.

As AF and thermal demagnetization preferentially remove LB components, remanent directions converge upon two antipodal HB directions: those that are consistently removed between 560 and 580°C by thermal demagnetization, and those above 50 mT by AF demagnetization. *In situ* site mean components show good clustering in a northerly declination, with steep negative inclinations or in antipode direction of southerly declination with a steep positive inclination (Fig. 20; Table 6).

The Upper Zone rocks all dip towards the centre of the Complex, with varying angles of between 10° and 18°. Upon stepwise unfolding, site mean HB directions (Fig. 19) showed a marginal increase in precision parameter κ from 42.4 to 51.2 and a slight decrease in α_{95} value from 8.6 to 7.8. This minor improvement was not sufficient to yield a statistically positive fold test. The reversal test of McFadden & Lowes (1981) found that the sites shared a common

Table 3. Main Zone, Western Lobe: Mean HB component of magnetization directions of each site *in situ*. Dec = mean declination; Inc = mean inclination; Strike/Dip = bedding orientation (right-hand convention); N = number of samples per site; α_{95} = 95 percent confidence circle around mean direction; κ = precision parameter.

Site	Dec	Inc	Strike	Dip	N	α_{95}	κ
10	146.20	86.30	268	25	9	3.1	271.37
11	258.50	85.80	279	26	9	2.8	298.13
12	126.60	89.10	273	16	9	2.2	537.21
13	9.90	69.90	268	12	9	4.7	199.97
14	12.20	77.20	266	10	9	2.1	604.36
15	35.10	81.90	275	12	8	1.6	1170.89
16	24.20	83.70	275	12	8	2.2	662.70
17	177.70	87.00	275	26	9	2.4	459.51
18	142.20	83.00	268	27	9	2.5	410.17
19	34.60	71.60	250	10	8	5.8	135.50
20	28.90	69.70	252	11	9	5.6	85.19
21	29.90	74.10	269	15	9	4.3	144.63
22	31.50	66.40	250	14	9	2.6	386.19
23	342.30	77.70	300	6	8	3.4	269.27
24	350.80	66.90	315	7	9	4.8	185.24
25	338.70	70.40	311	11	9	3.5	222.52
26	329.50	69.20	310	11	9	2.2	545.75
27	344.30	75.00	300	8	8	5.2	170.07
28a	345.10	74.40	354	10	9	5.9	171.57
28b	166.40	−55.60	354	10	9	9.1	71.23
29	328.90	72.80	312	11	8	2.9	369.55
30	329.20	69.10	312	10	8	2.4	658.06
31	332.50	73.60	306	11	8	2.2	645.67
32	325.90	79.10	307	11	8	1.5	1375.97
33	334.50	75.10	305	11	9	3.1	277.45
34	331.90	75.00	307	10	8	2.2	652.97
35	331.70	72.90	296	11	10	2.9	288.13
36	324.00	69.50	310	10	8	3.7	220.17
37	354.50	71.70	290	8	8	3.2	348.77
38	323.40	80.80	290	10	9	3.5	222.58
41	2.20	77.10	298	11	9	3	286.67

mean at 95% confidence level. The reversal test of McFadden & McElhinny (1990) also indicated a positive reversal test with a "C" classification, $\gamma_{\text{observed}} = 6.9$ and $\gamma_{\text{crit}} = 14.9$.

4.5 Northern Lobe Main Zone

Samples obtained from the Villa Nora section (sites 16–19) were unstable upon demagnetization and did not reveal any coherent components of magnetization, and have therefore not been included in the analysis of the Northern Lobe. Demagnetization experiments show the presence of two magnetization components (Fig. 21). Once again LB components identified in samples have directions that are random within sites and are typically removed at around 500°C or 30–40 mT.

After removal of LB components dual-polarity directions were isolated above 550°C or 50 mT (Fig. 21). HB components show reasonable grouping within-site (α_{95} around 6°). Mean site directions plot with SSW declination and steep negative inclination or antipodal to this (NNE declination and steep positive inclination; Fig. 22; Table 7).

Rocks to the south of Mokopane (Fig. 8) strike northeast and dip at angles of 15 to 27° west. To the north, the strikes change towards the northwest and eventually to due north, with westward dips of 10–45° (van der Merwe 1976). Upon stepwise unfolding of HB components, a slight increase in statistical precision parameter κ was observed from 48 to 67.6 and minor decrease in α_{95} value from 4.5° to 3.8°. The resulting increase in κ is not significant at the 95% confidence level (McElhinny 1964). Due to only one site possessing a negative primary inclination, only the reversal test of McFadden & Lowes (1981) could be applied to the data. It was found that the site shared a common mean at 95% confidence level.

Table 4. Main Zone, Eastern Lobe: Mean HB component of magnetization directions of each site *in situ*. See Table 3 for abbreviations.

Site	Dec	Inc	Strike	Dip	N	α_{95}	κ
1	220	−66.6	220	11	9	4.5	133.45
2a	220.5	−59.4	218	14	7	4.5	181.93
2b	209.2	−56.3	216	14	7	2.8	479.85
3	201.2	−47.7	210	15	14	6.4	39.15
8	36.2	61.9	169	10	8	2.8	405.98
42	35.9	64.8	195	12	9	2.4	477.92
43	30.8	61.4	190	11	10	2.4	420.08
44	48.5	61.4	194	10	8	2.8	389.93
45	30.2	67.9	205	10	9	1.6	1014.69
46	35.8	62.5	199	11	10	1.5	1099.84
47	39.5	62.7	193	11	9	1.1	2086.86
48	35.7	64.1	195	11	7	1.4	1910.6
49	32.8	66.7	197	10	8	0.9	4021.26
50	31.1	57.2	187	12	9	2.7	366.44
51	46.4	59.3	192	11	9	1.9	762.04
52	14.3	33.9	90	40	4	8.7	112.49
53	14.6	62.7	36	10	8	7.1	61.65
54	1.2	66.2	36	10	9	2.4	474.89
55	45.5	60.8	195	11	8	3.3	5550
56	32.9	57.7	181	10	5	7.5	104.64
58	45.5	60.8	181	12	8	3.3	8
59	358.2	75.1	160	10	6	4.4	236.6
61	203	−62.3	210	11	8	5	124.77
63	19.5	54.8	134	15	9	3.8	188.67
65	20.8	27.9	134	15	8	3.6	243.51
69	218.2	−71.1	216	14	8	4	195.24

Table 5. Critical Zone: Mean HB component of magnetization directions of each site *in situ*. See Table 3 for abbreviations.

Site	Dec	Inc	Strike	Dip	N	α_{95}	κ
4	43.5	59.2	182	12	7	8.2	25.68
66	200.5	−63.8	184	10	7	8.4	53.02
67	213.2	−68.1	184	10	6	7.1	90
68	9.8	45.8	145	11	6	6.8	195
H2	187.3	−57.1	182	10	10	3	265.56
B	172	−61.5	330	14	10	6.1	63.05
M	194	−73.6	184	10	11	4.5	101.83
H1	190.1	−52	182	10	7	4.3	193 030

5 INTERPRETATION

5.1 Main Zone, Western Lobe

Complete progressive demagnetization of samples has successfully removed minor LB components and identified HB components, which produce extremely well-clustered results for all sites. Thermal demagnetization spectra and TMA suggest that titanium (Ti)-poor titanomagnetite (TM) or nearly pure magnetite (maximum unblocking temperatures of 565–580°C and Curie temperatures at ∼580°C), probably in a single or pseudo-single domain state, is the bulk remanence carrier. Petrographic analysis further

Table 6. Upper Zone: Mean HB component of magnetization directions of each site *in situ*. See Table 3 for abbreviations.

Site	Dec	Inc	Strike	Dip	N	α_{95}	κ
5	212.5	−63	1.9	210	13	11	571.91
9	30	63.8	1.2	172	10	9	1897.72
39	161.6	−46.1	3.8	345	13	8	216.81
40	166.1	−50.3	3.2	342	12	8	304.18
57	14.4	65.8	4.2	156	10	8	175.44
60	192.9	−57.9	17.7	155	10	6	15.22
64	177.1	−65.1	3	134	8	9	287.94
70	168.3	−60.6	6.4	148	10	8	215.52

Table 7. Northern Lobe Main Zone: Mean HB component of magnetization directions of each site *in situ*. See Table 3 for abbreviations.

Site	Dec	Inc	Strike	Dip	N	α_{95}	κ
1	44.4	46.7	202	15	9	5.3	94.89
2	32.4	40.5	146	27	7	7.2	71.12
3	29.5	41.6	156	25	4	8.4	120.17
4	26.4	47.8	156	25	3	17.4	51.32
5	11.8	52.8	135	15	9	6.9	56.98
6	24.4	46.9	160	20	9	3.8	180.27
7	31.5	46.6	146	22	6	3.3	420.14
8	33.4	43.8	159	25	4	12.1	58.23
10	25.2	61.2	146	22	9	5.1	101.88
11	32.8	57.6	146	22	9	3.9	176.18
12	20.1	43.1	146	22	5	9.5	66.32
13	20.7	54.4	170	23	9	4.1	155.63
14	28.1	47.9	141	25	6	4.0	274.81
15	201.3	−47.8	141	25	8	4.8	134.40
20	54.8	65.1	169	20	9	2.9	306.99
21	58.1	65.5	209	26	9	2.9	312.93
22	41.6	63.7	169	24	9	3.3	243.67
23	61.9	65.4	180	16	8	2.9	373.32
24	46.4	68.1	187	21	3	13.0	90.60
25	32.4	53.2	168	30	6	12.5	29.60
26	20.4	43.4	170	20	3	12.4	99.64
27	32.3	66.3	180	25	4	4.8	367.53

strengthens these observations, revealing that the opaque mineralogy of the samples is dominated by magnetite.

A classic fold test yielded a statistically positive result, supporting a pre-fold magnetic signature of HB components, and indicates that at the time the western Main Zone passed through the Curie temperature of magnetite it was in a near horizontal position. A positive reversal test further attests that HB components are indeed primary, and that all sites were emplaced over a relatively short time span with little or no APW. Mean Zone HB statistics (with site 28b inverted to the same polarity as the other sites) are listed in Table 8.

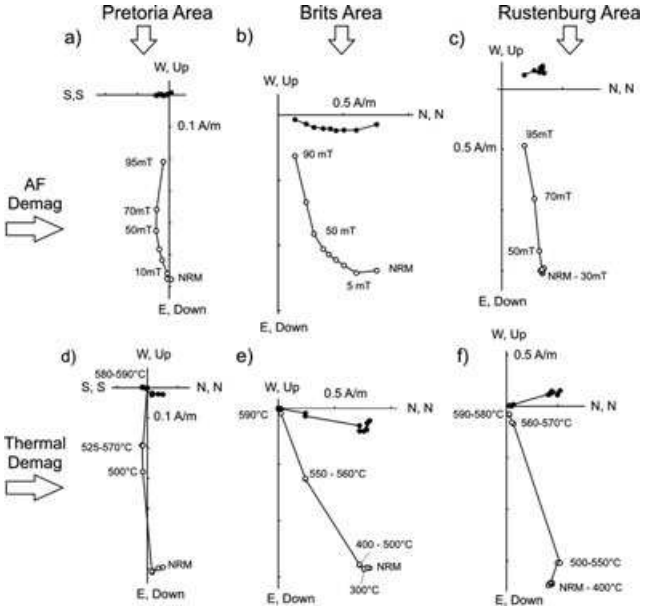

Figure 13. Typical examples of AF (a–c) and thermal demagnetization (d–f) of Main Zone samples from the three different geographical groups; Pretoria (a and d), Brits (b and e) and Rustenburg (c and f). Open (solid) symbols represent projections onto the vertical (horizontal) planes, respectively.

5.2 Main Zone, Eastern Lobe

The majority of NRM directions from the Eastern Lobe are directionally scattered, with the exception of sites obtained from dimension stone quarries. Progressive demagnetization successfully removed all minor LB components and allowed for the identification of well-defined HB components that produce extremely well-clustered results. During thermal demagnetization, it was revealed that samples had maximum unblocking temperatures at around 565–580°C, suggesting that Ti-poor TM or nearly pure magnetite is the bulk remanence carrier. This finding was further strengthened by TMA indicating a Curie temperature at ∼580°C and petrographic analysis revealing magnetite in the form of lamellae in plagioclase and pyroxene as the dominant opaque mineralogy. High coercivity attests to single or pseudo-single domain magnetite.

The presence of both polarities, and improved grouping after palaeo-horizontal corrections, point toward a primary magnetization being recorded by HB components. With this in mind, HB components were used to calculate a mean direction of magnetization for the eastern Main Zone (with negative inclinations inverted; Table 8).

5.3 Critical Zone

NRM directions from the Critical Zone show a reasonable grouping in two antipolar groupings. During demagnetization it was revealed

Table 8. Mean Zone statistics. N = number of sites per zone, α_{95} = 95 per cent confidence circle around the mean direction; κ = precision parameter; dp/dm = 95 per cent confidence ovals around the pole.

Zone	Dec	Inc	N	α_{95}	κ	Pole longitude	Pole latitude	dp	dm
Western Main Zone[#1]	1.1	66.9	32	2	169.27	15.5	28.2	2.7	3.3
Eastern Main Zone[#2]	14.7	63.8	26	3.3	83.2	18.3	40.5	2.7	5.2
Critical Zone[#3]	1.7	61.7	8	6.8	67.5	22.1	31	8.1	10.5
Upper Zone[#4]	174.8	−61.6	8	7.8	51.21	22.1	25.6	9.3	12
Northern Main Zone[#5]	359.8	66.1	22	3.8	67.55	17.5	28.8	5.1	6.2

Note: Mean sampling coordinates to calculate pole is [#1]25°S and 27.5°E, [#2–4].25°S and 29.7°E and [#5]24°S, 28.9°E.

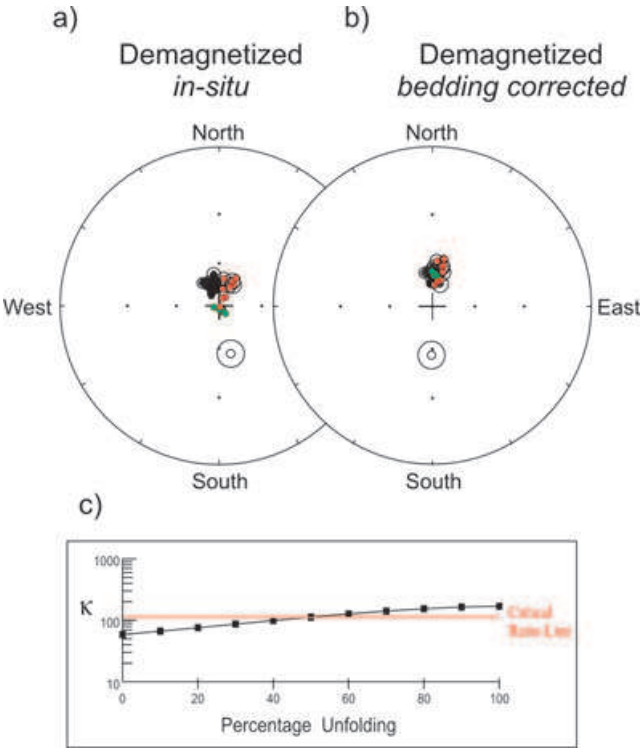

Figure 14. Site mean direction for Main Zone sites from the Western Lobe in both *in situ* (a) showing geographical location of sites, and bedding-corrected coordinates (b). Closed symbols denote positive inclination. Once again results have been colored based on geographic location, red symbols are from the Brits area, green from Pretoria area, black from the Rustenburg Area, (c) shows variation in precision parameter κ as a function of stepwise unfolding. The red line is the 'critical ratio-line' indicating the 95 per cent statistically significant level.

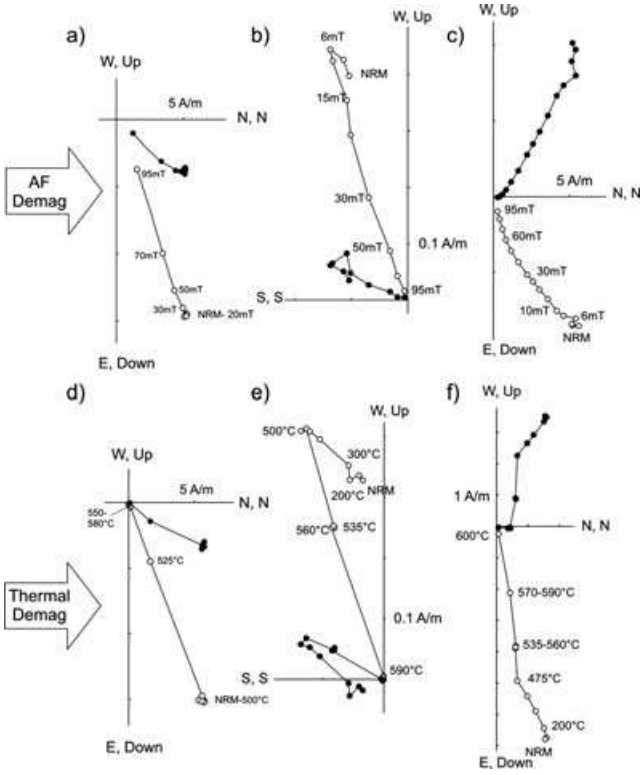

Figure 15. Characteristic examples of AF (a–c) and thermal (d–f) demagnetization of Eastern Lobe Main Zone samples. Samples from (a) and (d) have been acquired from dimension stone quarries and possess near univectorial demagnetization (i.e. single component of NRM) behaviour. Samples represented in (b), (c), (e) and (f) are from road cuttings and possess both LB and HB components.

that samples possess minor LB components that show no correlation with any known remanence direction for the area. Remanent directions converge upon HB components as demagnetization preferentially removed the less stable components, which displayed well-clustered results. HB components had maximum unblocking temperatures at around 565–580°C, suggesting that Ti-poor TM or nearly pure magnetite was the bulk remanence carrier. This finding was further strengthened by TMA indicating a Curie temperature at ~580°C.

The presence of both polarities in samples, and the slight improvement in grouping produced after palaeo-horizontal corrections points toward a primary magnetization being recorded by HB components. Although the Critical Zone was not significant at the 95% confidence level for the fold test of McElhinny (1964), the resulting pole position after bedding corrections plots closer in proximity to the other zones. Therefore, it is assumed that the Critical Zone acquired its magnetization whereas the layer was in a near horizontal position. The calculated mean direction of magnetization for the Critical Zone (with negative inclinations inverted) and pole position is listed in Table 8.

5.4 Upper Zone

In general, samples from the Upper Zone contained low temperature components that were successfully removed during progressive demagnetization to reveal the presence of high temperature

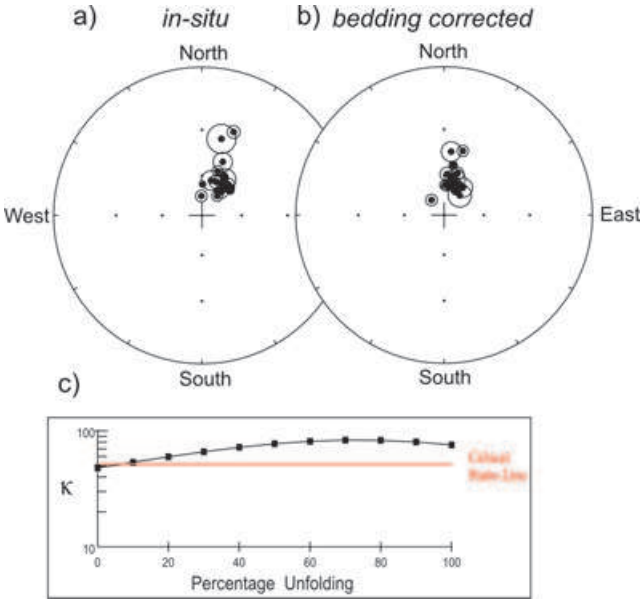

Figure 16. Site mean direction for Main Zone sites from the Eastern Lobe in both *in situ.* Sites with negative inclinations have been inverted to positive inclination (a), and bedding corrected coordinates (b). Closed symbols denote positive inclination, whereas open circles denote negative inclinations. (c) Shows variation in precision parameter κ as a function of stepwise unfolding. The red line is the 'critical ratio-line' indicating the 95% statistically significant level.

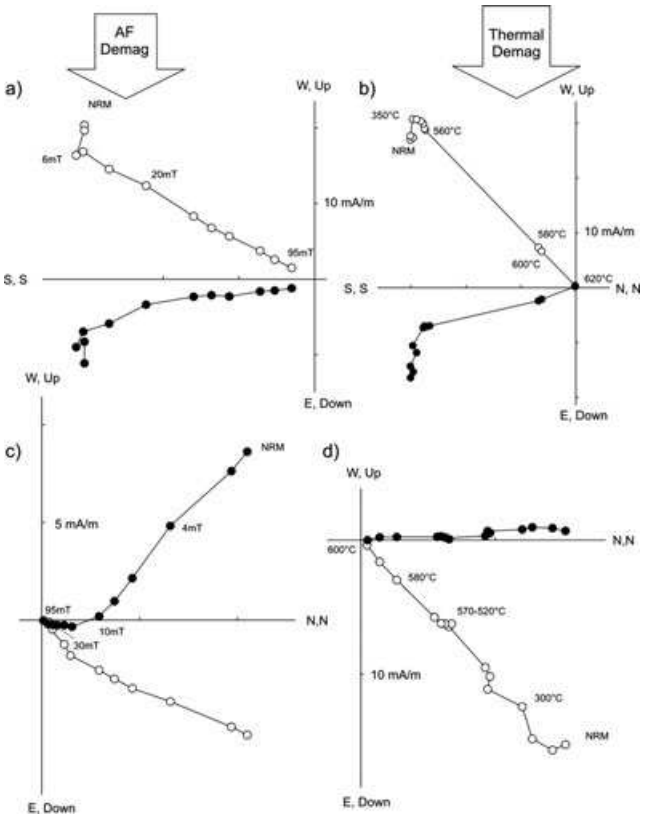

Figure 17. Typical Zijderveld diagrams from AF (a and c) and thermal demagnetization (b and d) of samples from the Critical Zone.

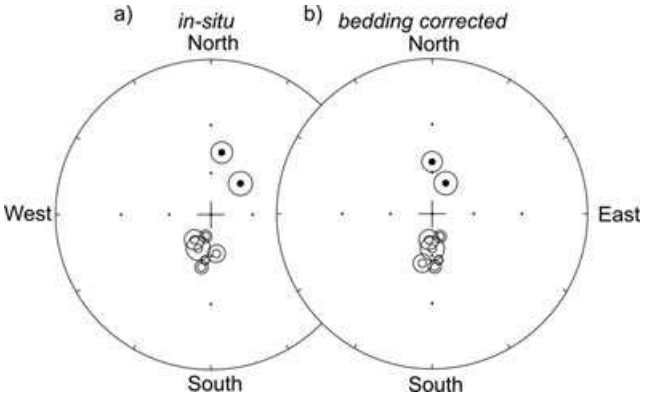

Figure 18. Site mean direction for Critical Zone sites *in situ* (a), and bedding corrected coordinates (b). Closed symbols denote positive inclination whereas open circles denotes negative inclinations.

components that produce extremely well-clustered results for sites. Both thermal demagnetization spectra and TMA suggest that Ti-poor magnetite or nearly pure magnetite (maximum unblocking temperatures at around 565–580 °C and Curie temperatures at ≈580 °C) is the bulk remanence carrier. This was further strengthened by petrographic analysis in which the opaque mineralogy of samples was dominated by magnetite.

Two positive reversal tests support that the HB components are the primary magnetic signature and that all sites were emplaced rather rapidly. Bedding-corrected data, although showing better grouping, were not significant at the 95% confidence level during the application of the positive fold test. However, the resulting palaeo-pole

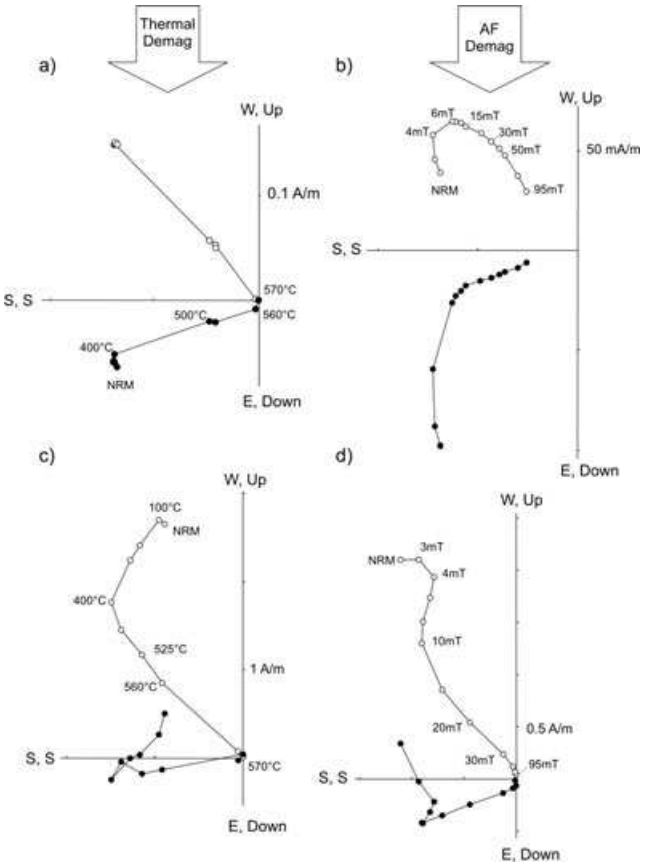

Figure 19. Typical Zijderveld plots for thermal (b and d) and AF (a and c) demagnetization of Upper Zone rocks. Generally two components of magnetization were identified as seen in (a) and (b). On the odd occasion three components were present in samples. However, due to the curved diagrams only two components were identified with certainty (c and d).

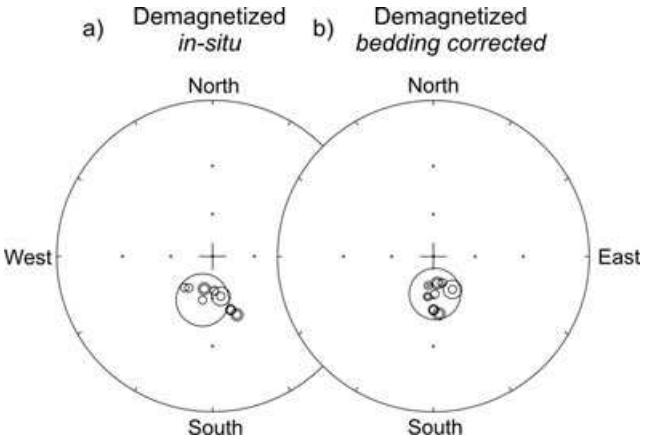

Figure 20. Site mean direction for Upper zone rocks in both *in situ* (a) and bedding corrected coordinates (b).

position obtained from bedding-corrected data shows a better association with poles calculated from the other Zones of the Bushveld and we have therefore concluded that the Upper Zone probably obtained its magnetization whereas the complex was horizontal. The mean HB components for all sites inverted to the same polarity are listed in Table 8.

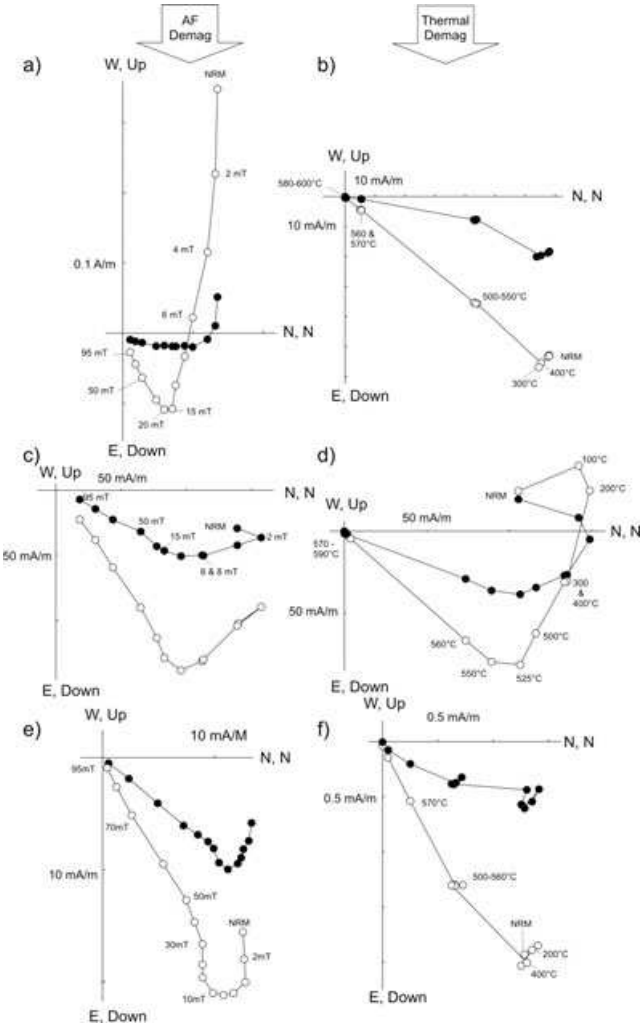

Figure 21. Typical Zijderveld diagrams from AF (a, c and e) and thermal demagnetization (b, d and f) of Main Zone samples from the Northern Lobe. Diagrams next to each other are from the same sites (e.g. a and b).

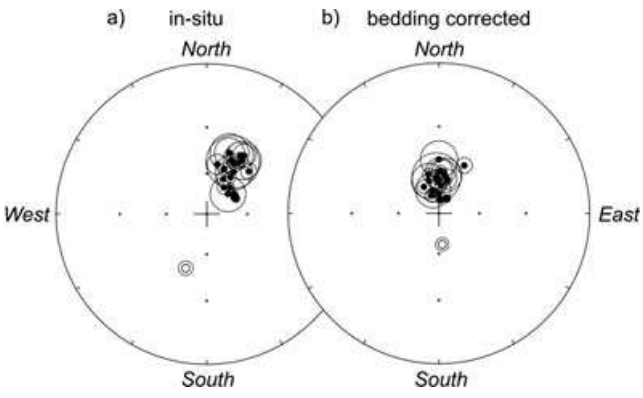

Figure 22. Site mean direction for Main Zone rocks from the Northern Lobe sites *in situ* (a), and bedding corrected coordinates (b).

5.5 Northern Lobe Main Zone

Both AF and thermal demagnetization removed low coercivity remanence that were scattered at site-level and have no correlation with any geological event. On completion of demagnetization remanent directions converge upon HB components that display well-clustered results. HB components had maximum unblocking temperatures at around 565–580°C, suggesting that Ti-poor TM or nearly pure magnetite is the bulk remanence carrier. This finding was further strengthened by TMA indicating a Curie temperatures at ≈ 580°C and petrographic analysis revealing magnetite in the form of lamellae in plagioclase and pyroxene as the dominate opaque mineralogy. Samples from the northern Main Zone contained both reversed and normal polarities. A reversal test indicated that the two polarities are of similar age, and argues for primary magnetization.

A slight improvement in sample clustering was obtained after palaeo-horizontal corrections were implemented. Although the findings of the fold test of McElhinny (1964) were not significant at the 95% confidence level, the resulting pole position plots closer in proximity to the other Zones. Therefore, it is assumed that the Zone acquired its magnetization whereas the layer was in a near horizontal position. The calculated mean direction of magnetization for the Northern Lobe with negative inclinations inverted is listed in Table 8.

6 CONCLUSION AND DISCUSSION

Samples from the Bushveld Complex behaved exceptionally well to both thermal and AF demagnetization, with two magnetization components (LB, HB) readily identified. LB components, although present in the majority of samples, mostly did not reveal any coherent directional pattern, and are typically removed below 300–500°C or 30–40 mT. Well-defined HB components are successfully identified at around 560–580°C and above 50 mT, indicating that the prime remanence carrier is possibly single or pseudo-single domain magnetite or Ti-poor titanomagnetite. This observation is further strengthened by Curie temperatures of ∼580°C, and the identification of magnetite occurring as needles or lamellae in pyroxene and plagioclase from petrographic analysis. The resulting HB components generate an extremely well grouped set of results for each Zone and both normal and reversed polarities are present (Fig. 23).

All Zones experienced an increase in precision parameter κ upon stepwise unfolding (Table 8, Fig. 24). Improved directional grouping is not only identified within Zones, but also as a whole. Although

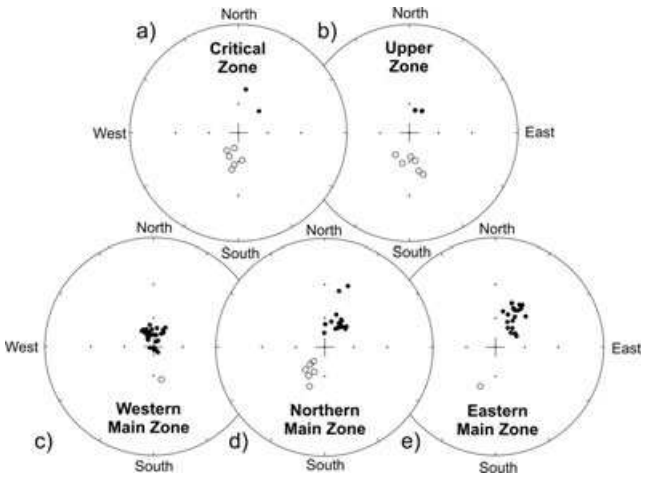

Figure 23. Mean *in situ* site HB components from all Zones of the Bushveld Complex. Upper Zone results are shown in (a), Critical Zone in (b), western Main Zone in (c), northern Main Zone in (d) and eastern Main Zone in (e).

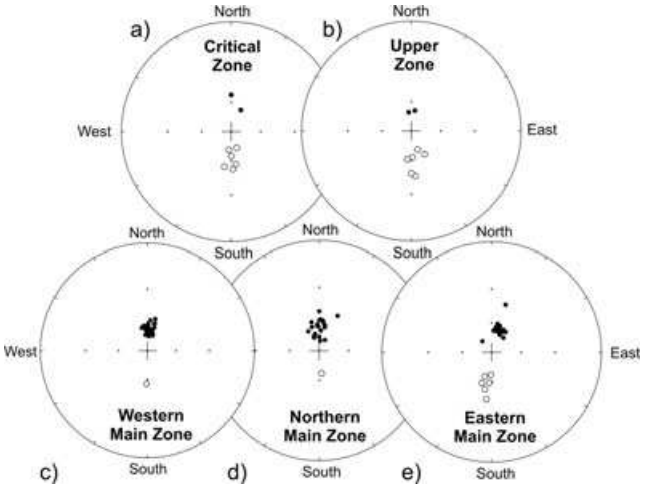

Figure 24. Mean bedding-corrected site HB components from all Zones of the Bushveld Complex. Upper Zone results are shown in (a), Critical Zone in (b), western Main Zone in (c), northern Main Zone in (d) and eastern Main Zone in (e).

only the western and eastern Main Zones statistically passed a classic fold test at the 95% confidence level (Table 9), we conclude that the Bushveld Complex was in a near-horizontal attitude when the blocking temperature of magnetite ($\leq$580°C) was reached. Positive reversal tests (Table 10) further suggest that the HB components must be primary.

The occurrence of igneous intrusions formed in a horizontal orientation before undergoing subsidence has been reported in a number of petrofabric and magnetic fabric studies: The Great Eucrite Gabbro intrusion of Ardnamurchan in NW Scotland has recently been interpreted by observations of magnetic fabric to have been emplaced in a horizontal orientation, and then at a later stage underwent considerable subsidence (O'Driscoll *et al.* 2006). Magnetic fabrics observed in the layered series of the Sonju Lake intrusion in northeast Minnesota, suggests a horizontal emplacement (Maes *et al.* 2006). Petrofabric analyses carried out on the Great Dyke revealed that pyroxenes from bronzitites exhibit well-developed linear lamination fabrics in the layering plane, with *c*-axes (longest axis) aligned parallel to the length of the Great Dyke. And *b*-axes are dominated by a strong central maximum perpendicular to the layering plane (Wilson 1992). Aligned elongate crystals are a characteristic feature of crescumulate type textures and have been interpreted to be diagnostic of *in situ* crystallization perpendicular to the floor of the magma chamber (Donaldson 1974; Lofgren & Donaldson 1975). The observed petrofabric findings suggest that the "Dyke" could have been emplaced in a horizontal orientation, before undergoing tilting. Although petrofabric/magnetic fabric findings have not been established for the Bushveld Complex, the above examples illustrate that it is likely for an igneous intrusions to have been emplaced in a horizontal attitude before undergoing subsidence, flexure or tilting.

It has been proposed that the load of the Bushveld Complex would induce flexure in the crust due to its large areal extent ($\sim$400 $\times$ 400 km), significant thickness (7–9 km) and high mean density ($\sim$3.05 g cm^{-3}) (Webb *et al.* 2004). However, even if the crust flexes by up to 6 km in the centre of the Bushveld Complex, because of its large size, the dip of the lithologies at the edge would only be $\sim$2° towards the centre. Thus the currently observed dips of between 10 and 25° are likely to have been acquired much later, consistent with the palaeomagnetic results.

Several polarity changes have been recorded throughout the Rustenburg Layered Suite (RLS, Fig. 25). Data from the Western Lobe appear to demonstrate a clear-cut relationship between Zones and polarity. Samples from both the Upper and Critical Zones are normally magnetized, whereas samples from the Main Zone are reversely magnetized with the exception of site 28b, a pyroxenite layer that is normally magnetized. However, gabbronorite samples obtained directly above ($\pm$5 cm) and below ($\pm$3 cm) this pyroxenite layer possess reversed magnetization and show no sign of overprint.

Magnetization recorded in the Eastern Lobe is similar to that in the Western Lobe, although the relationship between Zones and polarity is not as obvious. Within each Zone several polarities are present (Fig. 25), but overall the dominant magnetization for each Zone is the same as the Western Lobe with the Upper and Critical Zones possessing normal magnetization and the Main Zone being dominated by reversed magnetization.

From the available palaeomagnetic data it appears that the rocks of the Upper and Critical Zones of the Bushveld Complex cooled

Table 9. Summary of fold test results on all Zones, with precision parameter (κ) before and after application of bedding corrections.

Zone	Fold Test Result	κ-before	κ-after
Western Main Zone	Significant at 95 per cent confidence level	58.49	169.27
Eastern Main Zone	Significant at 95 per cent confidence level	42.7	83.2
Critical Zone	Improvement but not significant at 95 per cent confidence level	42.41	67.5
Upper Zone	Improvement but not significant at 95 per cent confidence level	42.41	51.21
Northern Main Zone	Improvement but not significant at 95 per cent confidence level	47.98	67.55

Table 10. Summary of reversal tests. γ_o is the observed angle between the two polarities and γ_c is the critical angle between the two mean directions.

Zone	Reversal test of *McFadden & Lowes (1981)*	Reversal test of *McFadden & McElhinny (1990)*
Western Main Zone	Passed at 95 per cent confidence level	*N/A:* only one reversal
Eastern Main Zone	Passed at 95 per cent confidence level	Passed: C $\gamma_o = 5.39$ $\gamma_c = 10.35$
Critical Zone	Passed at 95 per cent confidence level	Passed: C $\gamma_o = 5.71$ $\gamma_c = 16.11$
Upper Zone	Passed at 95 per cent confidence level	Passed: C $\gamma_o = 6.94$ $\gamma_c = 14.88$
Northern Zone	Passed at 95 per cent confidence level	*N/A*: only one reversal

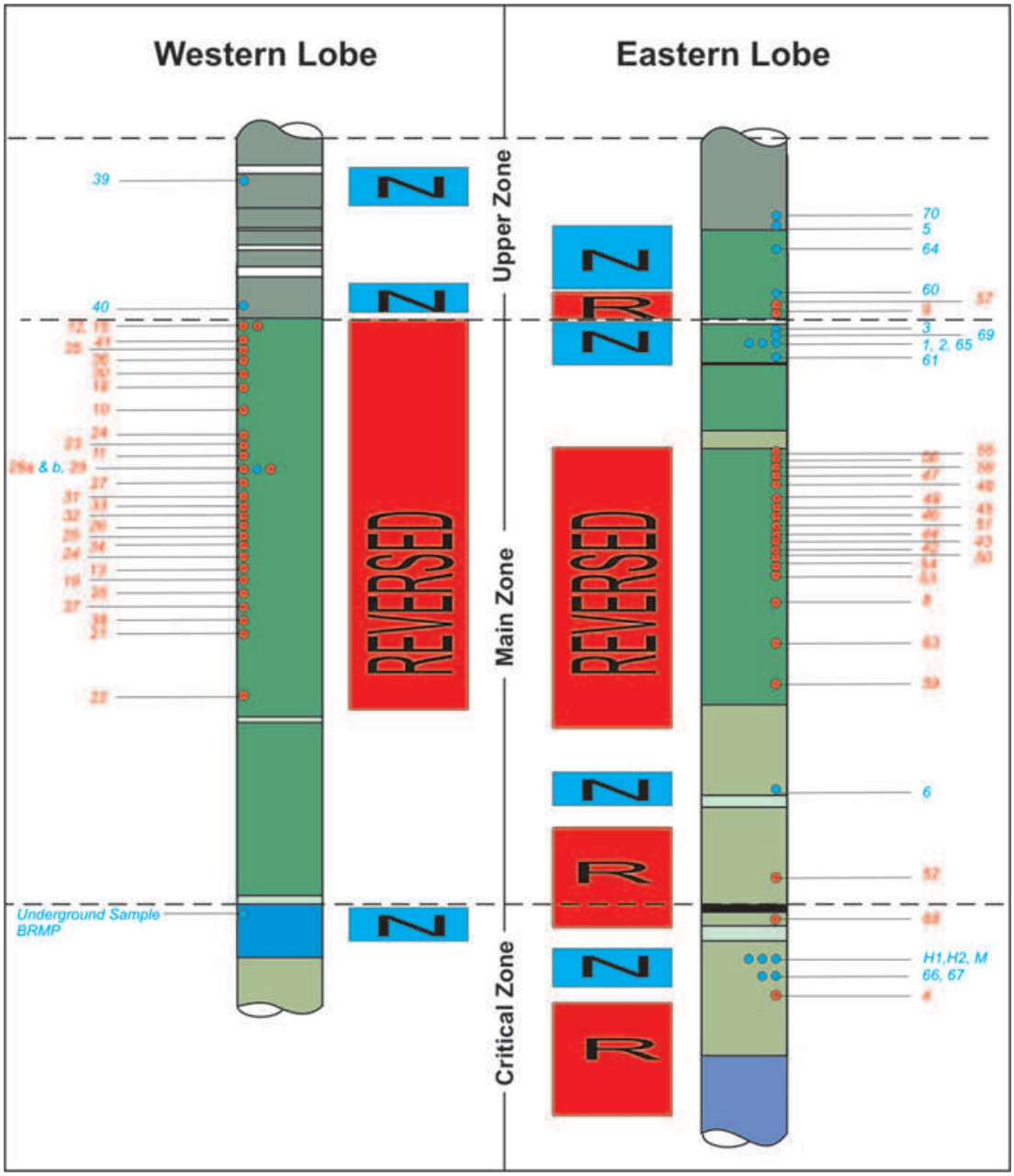

Figure 25. Simplified lithostratigraphic column of the Rustenburg Layered Suite in the Western Lobe and Eastern Lobe indicating the stratigraphic location and polarity of sampling sites. Red sites indicate a reversed polarity was recorded whereas blue represents a normal polarity. White areas in polarity column indicate polarity is unknown.

below the Curie Temperature for magnetite (~580°C) whereas the Earth's magnetic field was in a normal polarity and the rocks from the Main Zone acquired their magnetization during reversed polarity. During the cooling of each Zone, the Earth's magnetic field underwent two reversals in direction. The exact positions where polarity changed within Zones are not well defined, due to large gaps in the sampling coverage.

It should be noted that the observed change in polarity recorded in the Eastern Lobe above the Pyroxenite Marker (Figs 1 and 25), could provide evidence to strengthen the isotopic findings of Kruger (1994) in suggesting that a major magma influx occurred above the Pyroxenite Marker and hence represents a boundary between the Main and Upper Zones. Unfortunately, samples were not obtained directly above the Pyroxenite Marker but at a distance further up the stratigraphy, located above the Mottled Anorthosite layer (Figs 2 and 25). Therefore, it is possible that the Pyroxenite Marker might in fact possess the same polarity as the rest of the Main Zone. Further sampling closer to the Marker is needed to accurately determine this. With the available data, there is not enough credible information in proving the occurrence of new magma influx; a more in-depth and continuous study across the entire RLS is required to provide precise information.

Using the current data the only viable conclusions that can be inferred on the polarity findings is that during the cooling of the Bushveld Complex the rocks successfully recorded a number of reversals in the Earth's magnetic field.

With reversed and normal polarity sites within each zone sharing a common mean at the 95% confidence level, HB components

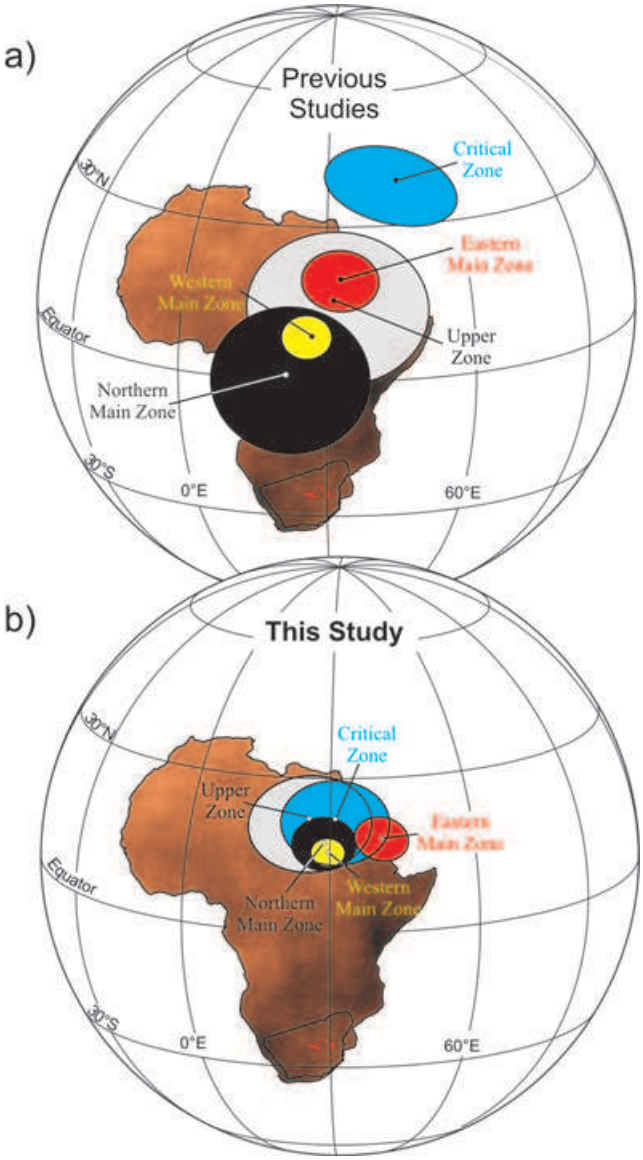

Figure 26. Comparison between old and new results for the Bushveld Complex. (a) Pole positions obtained by Hattingh (1983) and Hattingh & Pauls (1994). (b) Newly obtained pole positions from this study. Note the dramatic improvement in pole grouping compared with previous studies in (a).

were inverted to the same polarity and yielded a combined mean remanence direction, from which pole positions were calculated (Table 8, Fig. 26). Practically all pole positions for each zone overlap at the 95% significance (Fig. 26b) and produce well-clustered pole positions with a mean pole for the entire Bushveld Complex estimated to 16.2°N, 27.3°E (site-level) or 19.2°N, 030.8°E (Zone level). [Correction made after online publication 22 September 2009: the Zone level values have been corrected.] In contrast, earlier studies produced pole positions that were spread over ∼45° of arc (Fig. 26a), thereby suggesting considerable APW, and estimated to indicate a total emplacement age of ∼50 Myr. We attribute this to inadequate demagnetization in the earlier studies. Collectively our data indicate at least seven reversals in the Bushveld Complex (Fig. 25) – one of the fastest reversal rates in the geomagnetic field is documented for the past 5 Myr (∼5 per Myr), and thus a *minimum emplacement time* for all zones is estimated to 1.4 Myr.

The mean palaeomagnetic pole from the Bushveld Complex yield a palaeolatitude of ∼45° at eruption time (∼2054 Ma) but palaeogeographic implications of our findings together with a revised early Proterozoic APW path for the Kaapvaal Craton will be dealt with an a separate paper.

ACKNOWLEDGMENTS

We thank the South African and Norwegian Research Councils, the Geological Survey of Norway and Anglo American (Gordon Chunnett) for financial support and logistic assistance. We also thank Joe Meert and an anonymous referee for reviewing the manuscript.

REFERENCES

Ashwal, L.D., Webb, S.J. & Knoper, M.W., 2005. Magmatic stratigraphy in the Bushveld Northern Lobe: continuous geophysical and mineralogical data from the 2950 m Bellevue drillcore, *S. Afr. J. Geol.,* **108,** 199–232.

Buchanan, P.C., Reimold, W.U., Koeberl, C. & Kruger, F.J., 2002. Geochemistry of intermediate to siliceous volcanic rocks of the Rooiberg Group Bushveld Magmatic Province South Africa, *Contrib. Mineral. Petrol.,* **144,** 131–143.

Buick, I.S., Mass, R. & Gibson, R., 2001. Precise U-Pb titanite age constraints on the Bushveld Complex, South Africa, *J. geol. Soc. Lond.,* **158,** 3–6.

Caincross, B. & Dixon, R., 1995. *Minerals of South Africa,* Geological Soc. South Africa, Johannesburg.

Cawthorn, R.G. & Walraven, F., 1998. Emplacement and crystallization time for the Bushveld Complex, *J. Petrol.,* **39,** 1669–1687.

Donaldson, C.H., 1974. Olivine crystal types in harrisitic rocks of the Rhum pluton and Archean spinifex, *Geol. Soc. Am. Bull.,* **85,** 1721–1726.

Frick, C., 1973. The Sill phase and chill zone of the Bushveld Igneous Complex, *Trans. geol. Soc. S. Afr.,* **76,** 7–14.

Gough, D.J. & Van Niekerk, C.B., 1959. A study of the palaeomagnetism of the Bushveld gabbro, *Phil. Mag.,* **14,** 126–134.

Groeneveld, D., 1970. The structural features and the petrography of the Bushveld Complex in the vicinity of Stoffberg, Eastern Transvaal, *Geol. Soc. S. Afr. Spec. Public.,* **1,** 36–46.

Hattingh, P.J., 1983. *A palaeomagnetic investigation of the Layered mafic sequence of the Bushveld Complex*, University of Pretoria, Pretoria.

Hattingh, P.J., 1986a. The palaeomagnetism of the main zone in the western Bushveld Complex, *Earth planet. Sci. Lett.,* **79,** 441–452.

Hattingh, P.J., 1986b. The palaeomagnetism of the main zone of the eastern Bushveld Complex, *Tectonophysics,* **124,** 271–295.

Hattingh, P.J., 1986c. The palaeomagnetism of the Merensky Reef footwall rocks of the Bushveld Complex, *Trans. geol. Soc. S. Afr.,* **89,** 1–8.

Hattingh, P.J., 1989. Palaeomagnetism of the upper zone of the Bushveld Complex, *Tectonophysics,* **165,** 131–142.

Hattingh, P.J., 1995. Palaeomagnetic constraints on the emplacement of the Bushveld Complex, *J. Afr. Earth Sci.,* **21,** 549–551.

Hattingh, P.J., 1998. The Bushveld Complex and palaeomagnetism, in *Southern African Geophysical Review*, pp. 75–77, eds. Durrheim, R.J., Webb, S.J., 2. South African Geophysical Association.

Hattingh, P.J. & Pauls, N.D., 1994. New palaeomagnetic results from the northern Bushveld Complex of South Africa, *Precamb. Res.,* **69,** 229–240.

Hatton, C.J. & Von Gruenewaldt, G., 1987. The geological setting and petrogenesis of the Bushveld chromitite layers. in *Evolution of Chromium Ore Fields*, pp. 109–43, ed. Stowe, C.W., Van Nostr and Reinhold, New York.

Kirschvink, J.L., 1980. The least-squares line and plane and the analysis of paleomagnetic data, *Geophys. J. R. astr. Soc.,* **62,** 699–718.

Kruger, F.J., 1994. The Sr-isotopic stratigraphy of the western Bushveld Complex, *S. Afr. J. Geol.,* **97,** 393–398.

Lee, C.A., 1996. A review of the mineralization in the Bushveld Complex and some other layered mafic intrusions, in *Layered Intrusions.*

Developments in Petrology, pp. 103–145, ed. Cawthorn, R.G., Elsevier, Amsterdam.

Letts, S.A., 2007. The palaeomagnetic significance of the Bushveld Complex and related 2 GA magmatic rocks in ancient continental entities, *PhD thesis*. The University of the Witwatersrand, Johannesburg, 228 pp.

Lofgren, G.E. & Donaldson, C.H., 1975. Curved, branching crystals and differentiation in comb-layered ricks, *Contrib. Mineral. Petrol.,* **49,** 309–319.

Maes, S.M., Miller, J.D., Miller, T.D., Brown, P.E. & Tikoff, B., 2006. Magnetic Fabric if the Sonju Lake Intrusion, Northeastern Minnesota: Evidence for Internal Structure and Emplacement Dynamics, Philadelphia Annual Meeting (22–25 October 2006), Philadelphia, Pennsylvania.

McElhinny, M.W., 1964. Statistical significance of the fold test in palaeomagnetism, *Geophys. J. R. astr. Soc.,* **8,** 338–340.

McFadden, P.L. & Lowes, F.J., 1981. The discrimination of mean directions drawn from Fisher distributions, *Geophys. J. R. astr. Soc.,* **67,** 19–33.

McFadden, P.L. & McElhinny, M.W., 1990. Classification of the reversal test in palaeomagnetism, *Geophys. J. Int.,* **103,** 725–729.

Nomade, S., Renne, P.R. & Merkle, R.W., 2004. $^{40}Ar/^{39}Ar$ age constraints on ore deposition and cooling of the Bushveld Complex. South Africa, *J. geol. Soc. Lond.,* **161,** 411–420.

O'Driscoll, B., Troll, V.R., Reavy, R.J. & Turner, P., 2006. The Great Eucrite intrusion of Ardnamurchan, Scotland: re-evaluating the ring-dyke concept, *Geology,* **34,** 189–192.

SACS, 1980. Bushveld Complex, in *The stratigraphy of South Africa, Part I, Lithostratigraphy of the Republic of South Africa, South West Africa/Namibia and the Republics of Bophuthatswana, Transkei and Venda*, pp. 223–231, ed. K.L.E., Geological Survey of South Africa.

Scharlau, T.A., 1972. *Petrographische und petrologische Untersuchungen in der Haupt-Zon des ostlichen Bushvled-Komplexes, Distrct Groblersdal/Transvaal*, Universitat zu frnakfurt am Main.

Scoates, J.S. & Friedman, R.M., 2008. Precise age of the platiniferous Merensky Reef, Bushveld Complex, South Africa, by the U-Pb zircon chemical abrasion ID-TIMS technique, *Econ. Geol.,* **103,** 465–471.

Sharpe, M.R., 1981. *Evolution of the Bushveld magma chambers*, University of Pretoria, Research Report. 36.

Tankard, A.J., Jackson, M.P.A., Eriksson, K.A., Hobday, D.K., Hunter, D.R. & Minter, W.E.L., 1982. The Bushveld Complex: A Unique layered intrusion. The Vredefort Dome: Astrobleme or gravity-driven Diapir?, in *Crustal evolution of Southern Africa — 3.8 Billion Years of Earth History,* pp. 175–199, Springer, New York.

Torsvik, T.H., Briden, J.C. & Smethurst, M.A., 2000. Super-IAPD Interactive analysis of palaeomagnetic data, www.geodynamics.no/software.htm.

Van Der Merwe, M.J., 1976. The layered sequence of the Potgietersrus limb of the Bushveld Complex, *Econ. Geol.,* **71,** 1337–1351.

Walraven, F., 1985. Genetic aspects of the granophyric rocks of the Bushveld complex, *Econ. Geol.,* **80,** 1166–1180.

Walraven, F., 1997. *Geochronology of the Rooiberg Group, Transvaal Supergroup, South Africa, Economic Geology Research Unit*, University of the Witwatersrand, Johannesburg, South Africa, Information Circular, pp. 21.

Walraven, F. & Hattingh, E., 1993. Geochronolgy of the Nebo Granite, Bushveld Complex, *S. Afr. J. Geol.,* **96,** 31–41.

Webb, S.J., Nguuri, T.K., Cawthorn, R.G. & James, D.E., 2004. Gravity modelling of Bushveld Complex connectivity supported by southern African seismic experiment results, *S. Afr. J. Geol.,* **107,** 207–218.

Wilson, A., 1992. The geology of the Great Dyke, Zimbabew: crystallization, layering and cumulate formation in the P1 pyroxenite of Cyclic Unit 1 of the Darwendale Subchamber, *J. Petrol.,* **33,** 611–663.

APPENDIX A: ORIENTATION OF PALAEOMAGNETIC SAMPLES IN UNDERGROUND MINES

The orientation of palaeomagnetic samples from underground mines has previously been conducted by using a magnetic compass. Unfortunately in a mining area this method is not very reliable as a number of artefacts can easily deflect the readings. To ameliorate the problem of orientating samples, an instrument was created (Fig. A1) that could measure the angles from the strike of the rock to a survey pegs, and then through simple geometry the strike of the sample is determined. The device is made up of a laser pointer and protractor mounted on a piece of Perspex. To determine the strike of the sample, the angle from the strike of the rock to two survey pegs is required (angles $\hat{T}$ and $\hat{A}$) and the distance to one of the survey pegs (the distance to both pegs was recorded in this study to check results, distances b and c). The geometry of the underground sampling is shown in Fig. 1(b).

The exact coordinates of the survey pegs are also required (these were obtained from the mine). From the coordinates, the angle between true north and the azimuth of line connecting the two pegs is determined (angle $\hat{x}$) as well as the distance between the two pegs (distance a).

Figure A1. Orientation device used to accurately orientate samples underground. The flat end of the device is placed along the strike of the rock and the laser pointer is then pointed towards the survey peg, where the bearing is read off.

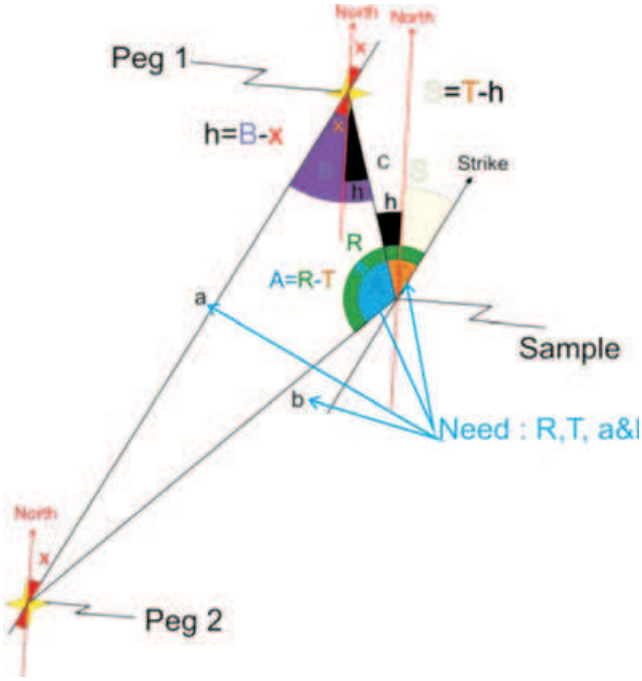

Figure A2. The geometry of the underground sampling.

From the measured angles $\hat{R}$ and $\hat{T}$, the internal angle $\hat{A}$, is determined by

$$\hat{A} = \hat{R} - \hat{T}.$$

If the distance b was measured then the angel $\hat{B}$ is calculated by use of the Sine Rule,

$$\hat{B} = \arcsin\left(b \sin \frac{\hat{A}}{a}\right).$$

Once $\hat{B}$ had been calculated the angel $\hat{h}$ is determined by

$$\hat{h} = |\hat{B} - \hat{x}|$$

and finally the strike of the sample S is calculated by

$$\hat{S} = |\hat{T} - \hat{h}|$$

or simply by placing all equations together

$$\hat{S} = \left|\hat{T} - \left(\left|\left[\arcsin\left(b \sin \frac{\hat{A}}{a}\right)\right] - x\right|\right)\right|$$

if the distance c was measured then the strike can be determined using the following equation:

$$\hat{S} = \left|\hat{T} - \left(\left|\left[\arcsin\left(c \sin \frac{\hat{A}}{a}\right)\right] - x\right|\right)\right|.$$